

Jahn-Teller magnets

Alexander Moskvina¹

¹*Ural Federal University, 620083 Ekaterinburg, Russia*

arXiv:2306.06612v1 [cond-mat.str-el] 11 Jun 2023

Abstract

A wide class of materials with different crystal and electronic structures from quasi-two-dimensional unconventional superconductors (cuprates, nickelates, ferropnictides/chalcogenides, ruthenate SrRuO_4), 3D systems as manganites RMnO_3 , ferrates $(\text{CaSr})\text{FeO}_3$, nickelates RNiO_3 , to silver oxide AgO are based on Jahn-Teller $3d$ and $4d$ ions. These unusual materials called Jahn-Teller (JT) magnets are characterized by an extremely rich variety of phase states from non-magnetic and magnetic insulators to unusual metallic and superconducting states. The unconventional properties of the JT-magnets can be related to the instability of their highly symmetric Jahn-Teller "progenitors" with the ground orbital E -state to charge transfer with anti-Jahn-Teller $d-d$ disproportionation and the formation of a system of effective local composite spin-singlet or spin-triplet, electronic or hole S -type bosons moving in a non-magnetic or magnetic lattice. We consider specific features of the anti-JT-disproportionation reaction, properties of the electron-hole dimers, possible phase states of JT-magnets, effective Hamiltonians for single- and two-band JT-magnets, and present a short overview of physical properties for actual JT-magnets.

INTRODUCTION

We call Jahn-Teller (JT) magnets compounds based on Jahn-Teller $3d$ - and $4d$ -ions with configurations of the $t_{2g}^{n_1}e_g^{n_2}$ type in a highly symmetrical octahedral, cubic, or tetrahedral environment and with ground state orbital E -doublet. These are compounds based on tetra-complexes with the configuration d^1 (Ti^{3+} , V^{4+}), low-spin (LS) configuration d^3 (V^{2+} , Cr^{3+} , Mn^{4+}), and high-spin (HS) configuration d^6 (Fe^{2+} , Co^{3+}), octa-complexes with HS-configuration d^4 (Cr^{2+} , Mn^{3+} , Fe^{4+} , Ru^{4+}), low-spin configuration d^7 (Co^{2+} , Ni^{3+} , Pd^{3+}), as well as octa-complexes with configuration d^9 (Cu^{2+} , Ni^{1+} , Ag^{2+}) (see Table I). The class of JT-magnets includes a large number of promising materials that are the focus of modern condensed matter physics, such as RMnO_3 manganites, $(\text{Ca,Sr})\text{FeO}_3$ ferrates, ruthenates RuO_2 , $(\text{Ca,Sr})\text{RuO}_3$, $(\text{Ca,Sr})_2\text{RuO}_4$, a wide range of ferropnictides (FePn) and ferrochalcogenides (FeCh), RNiO_3 3D nickelates, 3D- cuprate KCuF_3 , 2D cuprates (La_2CuO_4 , ...) and nickelates RNiO_2 , silver-based compounds (AgO , AgF_2) (see Table I).

Among these materials, it is necessary to highlight JT magnets with charge transfer, in particular, disproportionation, which have a rich spectrum of unique properties from various types of magnetic and charge ordering to metal-insulator transitions and superconductivity.

Interestingly, the choice of cuprates as promising superconducting materials and the discovery of high-temperature superconductivity (HTSC) [1] were stimulated precisely by the outstanding Jahn-Teller character of Cu^{2+} ions.

Many authors considered disproportionation as a mechanism ("negative- U " model) leading to "glueless" superconductivity of a system of local electron pairs, or composite bosons (see, e.g., Refs. [2–19]). The concept of superconductivity as a Bose-Einstein condensation (BEC) of local composite bosons as two electrons bound in real space was introduced by Ogg Jr. in 1946 [20] and developed by Schafroth in 1954-55 [21]. However, due to the triumph of the BCS (Bardeen-Cooper-Schrieffer) theory, the idea of local composite bosons and preformed pairs was practically forgotten for many years. The discovery of HTSC cuprates in 1986 revived interest in the idea of local pairing [22], especially since this idea has been supported by K. A. Mueller, the discoverer of HTSC [23]. Now there is convincing experimental evidence that the local pairing of carriers takes place well above T_c at least in underdoped cuprates [24]. At the same time, until now, one way or another, the HTSC theory has been dominated by the approaches based on the BCS paradigm, i.e, on the representations of the BCS model theory applicable to the description of typical low-temperature superconductors. This is largely due to the fact that an appealingly simple picture of the preformed pairs and BEC superconductivity in cuprates seemingly came to be at odds with a number of experimental observations of the typical Fermi liquid behavior, and notably with indications that a well-defined Fermi surface (FS) exists, at least in overdoped cuprates, the thermal and electrical conductivity were found to follow the standard Wiedemann-Franz law, quantum oscillations have been observed as well in various cuprates [25].

However, this contradictory behavior can be easily explained if we take into account the possibility of separating the superconducting BEC phase and the normal Fermi-liquid phase. Indeed, recently Pelc *et al.* [26] have introduced a phenomenological model of a "local phase separation" wherein two electronic subsystems coexist within the unit cell: itinerant and localized holes, with the p holes introduced via doping always being itinerant while pairing is associated with the localized holes. In fact, they argue that the Fermi liquid subsystem in cuprates is responsible for the normal state with angle-resolved photoemission spectra (ARPES), magnetic quantum oscillations, and Fermi arcs, but not for the unconventional superconducting state. In other words, *cuprate superconductivity is not related to the doped hole pairing*, the carriers which exhibit the Fermi liquid behaviour are not the ones that

give rise to superconductivity. However, the authors could not elucidate the nature of local pairing to be a central point of the cuprate puzzle.

The disproportionation scenario, especially popular in the "chemical" community ("chemical" way to superconductivity), was addressed earlier by many authors, however, by now it was not properly developed theoretically, and perhaps that is why it has not yet been a worthy competitor to the traditional BCS approach.

Previously, we proposed a mechanism for anti-Jahn-Teller disproportionation [27] with the formation of a system of local composite spin-triplet bosons and unconventional bosonic superconductivity in $3d$ JT magnets. This mechanism indicated, in particular, the spin-triplet superconductivity of ferropnictides and ferrochalcogenides, which was predicted back in 2008 [28]. Over the past years, new results have been obtained in the study of JT magnets based on both $3d$ and $4d$ ions, as well as new arguments both for and against spin-triplet superconductivity.

In this paper, we develop a model of "anti-Jahn-Teller" disproportionation into a wider class of Jahn-Teller magnets, including $4d$ magnets (ruthenates, silver compounds) and 2D nickelates RNiO_2 , and show that all of them can be described within a single scenario. In Sec. II, we present a more detailed description of the anti-JT disproportionation for JT-magnets and formation of effective local composite bosons. In Secs. III and IV we consider electron-hole (EH) dimers as specific "disproportionation quanta", their electron and spin structure. Sec. V provides a brief overview of the possible phase states for JT magnets. Secs. VI and VII present the effective Hamiltonians of single- and two-band JT magnets with a brief overview of the properties of real JT magnets. A brief conclusion is given in Sec. VIII.

ANTI-JAHN-TELLER DISPROPORTIONATION

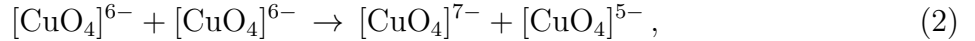
The lifting of the orbital E -degeneracy in the high-symmetry "progenitor" JT-magnets can be associated both with the specifics of the crystal structure, as, for example, in "apex-free" 2D cuprates (Nd_2CuO_4) and RNiO_2 nickelates, and with the conventional Jahn-Teller effect, which, as a rule, leads to the formation of a low-symmetry insulating antiferromagnetic (La_2CuO_4 , KCuF_3 , LaMnO_3) or ferromagnetic (K_2CuF_4) phase. A competing mechanism for removing orbital degeneracy in JT magnets considered above is "anti-Jahn-Teller",

”symmetric” d - d -disproportionation according to the scheme



assuming the formation of a system of bound or relatively free electronic d^{n+1} and hole d^{n-1} centers, differing by a pair of electrons/holes. Formally, an electron/hole center can be represented as a hole/electron center with a pair of electrons/holes d^2/\underline{d}^2 localized at the center. In other words, a disproportionate system can be formally represented as a system of effective local spin-singlet or spin-triplet composite electron/hole bosons ”moving” in the lattice of hole/electron centers. Note that in frames of the toy model (1) the disproportionation energy Δ_{dd} formally coincides with the energy of local correlations U_{dd} , which gives reason to associate symmetric d - d -disproportionation with the negative- U phenomenon.

Obviously, in systems with strong d - p -hybridization (cation-anion covalence), the disproportionation reaction (1) must be written in a ”cluster” language, for example, as for CuO_4 clusters in the CuO_2 cuprate planes



instead of



The cation-ligand cluster representation of the $d^n, d^{n\pm 1}$ -centers immediately indicates the important role of the so-called ”breathing mode” of the ligand displacements in perovskite-type JT-magnets with corner-shared coupling of neighboring octahedral d -centers. The displacement amplitude of the common ligand for two centers during disproportionation can reach values greater than of 0.1 Å due to the large difference in the cation–ligand separation for the electron and hole centers. Thus, the Cu-O separation for CuO_4 -centers in cuprates increases by 0.2 Å from the hole $[\text{CuO}_4]^{5-}$ to electron $[\text{CuO}_4]^{7-}$ center [29]. Softening of the breathing mode is considered an indication of disproportionation. The electron-lattice interaction leads to the stability of the electron and hole centers in the lattice of the parent system with the ground states of all three centers – the electron, parent, and hole one corresponding to different values of the local breathing configuration coordinate $Q_{A_{1g}}$: $+Q_0$, 0, $-Q_0$, respectively.

Note that in any case, ”symmetric” d - d -disproportionation, in contrast to ”asymmetric”, ”single-center”, d - p -disproportionation [30–32] has a two-center character, although it may

include d - p -transfer between clusters. Obviously, symmetric d - d disproportionation will be energetically more favorable in "progenitor" Mott-Hubbard JT magnets, and vice versa, asymmetric d - p -disproportionation will be more energetically favorable in charge-transfer (CT) insulators ("negative charge transfer" materials).

It is worth noting that all the JT-magnets are characterized by empty, half-filled or fully filled t_{2g} -subshell with orbitally non-degenerate, or S -type ground state, and with only one e_g -electron or hole. Obviously, the anti-JT-disproportionation implies the e_g - e_g intersite transfer with the formation of the empty, half-filled or fully filled e_g -subshells with the S -type ground state for the electron and hole centers. In all cases, we arrive at relatively stable S -type configurations of electron and hole centers. For all JT magnets, the anti-JT disproportionation reactions can be written as follows

$$tetra\ d^1 : e_g^1 + e_g^1 \xrightarrow{e_g} \left\{ \begin{array}{l} e_g^0 + e_g^0 e_g^2 \\ e_g^0 e_g^2 + e_g^0 \end{array} \right\}; \quad (4)$$

$$tetra\ d^3 : e_g^3 + e_g^3 \xrightarrow{e_g} \left\{ \begin{array}{l} e_g^4 + e_g^4 e_g^2 \\ e_g^4 e_g^2 + e_g^4 \end{array} \right\}; \quad (5)$$

$$octa\ d^4 : t_{2g}^3 e_g + t_{2g}^3 e_g \xrightarrow{e_g} \left\{ \begin{array}{l} t_{2g}^3 + t_{2g}^3 e_g^2 \\ t_{2g}^3 e_g^2 + t_{2g}^3 \end{array} \right\}; \quad (6)$$

$$tetra\ d^6 : e_g^3 t_{2g}^3 + e_g^3 t_{2g}^3 \xrightarrow{e_g} \left\{ \begin{array}{l} e_g^4 t_{2g}^3 e_g^2 + e_g^4 t_{2g}^3 \\ e_g^4 t_{2g}^3 + e_g^4 t_{2g}^3 e_g^2 \end{array} \right\}; \quad (7)$$

$$octa\ d^7 : t_{2g}^6 e_g + t_{2g}^6 e_g \xrightarrow{e_g} \left\{ \begin{array}{l} t_{2g}^6 + t_{2g}^6 e_g^2 \\ t_{2g}^6 e_g^2 + t_{2g}^6 \end{array} \right\}; \quad (8)$$

$$octa\ d^9 : t_{2g}^6 e_g^3 + t_{2g}^6 e_g^3 \xrightarrow{e_g} \left\{ \begin{array}{l} t_{2g}^6 e_g^4 e_g^2 + t_{2g}^6 e_g^4 \\ t_{2g}^6 e_g^4 + t_{2g}^6 e_g^4 e_g^2 \end{array} \right\}. \quad (9)$$

Obviously, for JT magnets with the on-site progenitor configurations e_g^1 , $t_{2g}^3 e_g^1$, $t_{2g}^6 e_g^1$ we are dealing with the transfer of the e_g -electron, while for configurations $e_g^3 t_{2g}^3$ and $t_{2g}^6 e_g^3$ it is correct to speak of the e_g -hole (\underline{e}_g) transfer. Thus for these configurations we arrive at a doublet of ionic states with site-centred charge order, or two centers that differ in the transfer (exchange) of two e_g -electrons or two e_g -holes, respectively, that can be thought of as effective local composite bosons. For the centers with high (octahedral, tetrahedral) symmetry these effective bosons will be described by the low-energy Hund configuration $e_g^2; {}^3A_{2g}$ or $\underline{e}_g^2; {}^3A_{2g}$.

It should be noted that effective bosons cannot be considered as conventional quasiparticles, they are an indivisible part of many-electron configurations.

All JT-magnets can be conditionally divided into the "single-band" and "two-band" ones. In single-band JT-magnets with the configurations d^1 , d^3 , d^7 , and d^9 , effective electron (d^1 , d^7) or hole (d^3 , d^9) composite bosons move in the lattice of ions with completely filled shells, while in two-band JT-magnets (d^4 , d^6) the lattice includes ions with half filled t_{2g} -subshell.

The optimal configurations and spin of the composite boson, as well as the orbital state and local spin of the lattice, formed as a result of anti-JT disproportionation in JT magnets with the $3d^n$ configuration, as well as some $4d^n$ JT configurations, are given in the fourth and fifth columns of Table I. Note that in all cases the complete disproportionation leads to a system of composite bosons with the concentration of 1/2, or half-filling.

ELECTRON-HOLE DIMERS

Pair of bound electron and hole centers, an EH dimer, is a kind of "disproportionation quantum". In Mott-Hubbard insulators, EH dimers are low-energy metastable charge excitations above the ground state or may be the result of the self-trapping of the d - d CT-excitons [33].

The two electron/hole charge exchange reaction in EH dimer

$$d_1^{n+1} + d_2^{n-1} \xleftrightarrow{e_g^{2,3} A_{2g}} d_1^{n-1} + d_2^{n+1}, \quad (10)$$

is controlled by the effective local boson transfer integral

$$t_B = \langle d_1^{n+1} d_2^{n-1} | \hat{H}_B | d_1^{n-1} d_2^{n+1} \rangle, \quad (11)$$

where \hat{H}_B is an effective two-particle (bosonic) transfer Hamiltonian and we assume ferromagnetically ordered spins of the two centers. As a result of this quantum process the bare ionic states with site-centered charge order and the same bare energy E_0 transform into two EH-dimer states with an indefinite valence and bond-centred charge-order

$$|\pm\rangle = \frac{1}{\sqrt{2}} (|d_1^{n+1} d_2^{n-1}\rangle \pm |d_1^{n-1} d_2^{n+1}\rangle) \quad (12)$$

with the energies $E_{\pm} = E_0 \pm t_B$. In other words, the exchange reaction restores the bare charge symmetry. In both $|\pm\rangle$ states the on-site number of d -electrons is indefinite with

quantum fluctuations between $(n+1)$ and $(n-1)$, however, with a mean value n . Interestingly that, in contrast with the ionic states, the EH-dimer states $|\pm\rangle$ have both a distinct electron-hole and inversion symmetry, even parity (s -type symmetry) for $|+\rangle$, and odd parity (p -type symmetry) for $|-\rangle$ states, respectively. The both states are coupled by a large electric-dipole matrix element:

$$\langle +|\hat{\mathbf{d}}|-\rangle = 2eR_{12}, \quad (13)$$

where R_{12} is a 1 – 2 separation. The two-particle transport (10) can be realized through two successive one-particle processes with the e_g -electron transfer as follows

$$d_1^{n+1} + d_2^{n-1} \xrightarrow{e_g} d_1^n + d_2^n \xrightarrow{e_g} d_1^{n-1} + d_2^{n+1},$$

hence the two-particle transfer integral t_B can be evaluated as follows:

$$t_B = -t_{e_g e_g}^2/U \approx -J_{kin}(e_g e_g), \quad (14)$$

where $t_{e_g e_g}$ is one-particle transfer integral for e_g electron, U is a mean transfer energy. It means that the two-particle bosonic transfer integral can be directly coupled with the kinetic e_g -contribution $J_{kin}(e_g e_g)$ to Heisenberg e_g - e_g exchange integral. Both t_B and $J_{kin}(e_g e_g)$ are determined by the second order one-particle transfer mechanism. It should be noted that negative sign of the two-particle CT integral t_B points to the energy stabilization of the s -type EH-dimer state $|+\rangle$.

Second, one should emphasize once more that the stabilization of EH-dimers is provided by a strong electron-lattice effect with a striking intermediate oxygen atom polarization and displacement concomitant with charge exchange. In a sense, the EH-dimer may be addressed to be a bosonic counterpart of the Zener Mn^{4+} - Mn^{3+} polaron [34]. It is no wonder that even in a generic disproportionated system BaBiO_3 instead of simple checker-board charge ordering of Bi^{3+} and Bi^{5+} ions we arrive at a CDW (charge density wave) state with the alteration of expanded $\text{Bi}^{(4-\rho)+}\text{O}_6$ and compressed $\text{Bi}^{(4+\rho)+}\text{O}_6$ octahedra with $0 < \rho \ll 1$ [35]. Enormously large values of oxygen thermal parameters in BaBiO_3 [36] evidence a great importance of dynamical oxygen breathing modes providing some sort of a "disproportionation glue". Sharp rise of the oxygen thermal parameter in the high-temperature O phase of LaMnO_3 [37] or in several "competing" phases found by Huang *et al.* [38] as compared with the bare AFI phase is believed to be a clear signature of the high-temperature manganese disproportionation [39].

Actually we deal with an EH-dimer to be a dynamically charge fluctuating bipolaronic system of coupled electron d^{n+1} and hole d^{n-1} centers having been glued in a lattice due to a specific local expansion/contraction mode of neighboring clusters (half-breathing, or breathing mode) and strong electron-lattice polarization effects.

SPIN STRUCTURE OF EH-DIMERS

Let's apply to spin degrees of freedom which are of great importance for magnetic properties of EH-dimers as nucleation centers for a rich variety of different phases. First of all, we note that the structure of EH-dimers is significantly different in single- and two-band JT magnets. In EH-dimers of JT magnets based on d^1 , d^7 , and d^9 configurations, the spin-triplet boson "moves" along spinless centers (see Table 1), which leads to a trivial spin structure of the dimer. A more complicated situation is realized for EH-dimers of JT magnets based on d^4 and d^6 configurations, where the spin-triplet boson "moves" through the $d^3(t_{2g}^3)$ -centers with spin 3/2 (see Table 1).

The total spin moment of these EH-dimers is $\mathbf{S} = \mathbf{S}_1 + \mathbf{S}_2$, where \mathbf{S}_1 ($S_1 = 5/2$) and \mathbf{S}_2 ($S_2 = 3/2$) are spins of d^5 and d^3 (d^5 and d^3) configurations, respectively, so the total spin magnitude S takes the values 1, 2, 3, 4. In nonrelativistic approximation the spin structure of the EH-dimer in the bare ionic state d^5-d^3 (d^3-d^5) with site-centered charge order will be determined by isotropic Heisenberg exchange coupling

$$V_{ex} = J(d^5 d^3) (\mathbf{S}_1 \cdot \mathbf{S}_2), \quad (15)$$

with $J(d^5 d^3)$ being a d^5-d^3 (d^3-d^5) (super)exchange integral. However, the two site-centered states d^5-d^3 and d^3-d^5 are coupled by the two-particle charge transfer characterized by a respective transfer integral which depend on spin states as follows:

$$\langle \frac{5}{2} \frac{3}{2}; SM | \hat{H}_B | \frac{3}{2} \frac{5}{2}; SM \rangle = \frac{1}{20} S(S+1) t_B, \quad (16)$$

where t_B is a spinless transfer integral. Making use of this expression we can introduce an effective spin-operator form for the boson transfer as follows:

$$\hat{H}_B^{eff} = \frac{t_B}{20} [2(\hat{\mathbf{S}}_1 \cdot \hat{\mathbf{S}}_2) + S_1(S_1+1) + S_2(S_2+1)], \quad (17)$$

which can be a very instructive tool both for qualitative and quantitative analysis of boson transfer effects. Thus, the effective transfer integral of the composite boson strongly depends

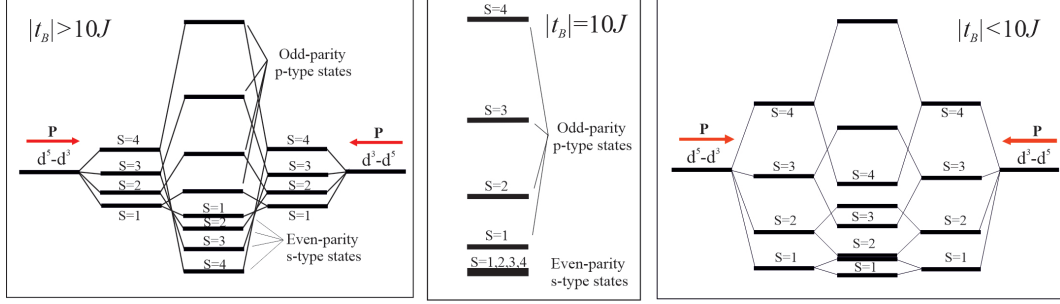


FIG. 1. (Color online) Spin structure of the EH-dimer, or self-trapped CT exciton with a step-by-step inclusion of one- and two-particle charge transfer. Arrows point to electric dipole moment for bare site-centered dimer configurations.

on the spin state of the electron-hole pair, falling tenfold as the total spin of the pair changes from $S=4$ to $S=1$. In particular, we arrive at a strong, almost twofold, suppression of effective transfer integral in paramagnetic phase as compared with its maximal value t_B for a ferromagnetic ordering ($S=4$).

Both conventional Heisenberg exchange coupling d^5-d^3 (d^3-d^5) and unconventional two-particle bosonic transfer, or bosonic double exchange can be easily diagonalized in the total spin S representation so that for the energy of the EH-dimer we arrive at

$$E_S = \frac{J(d^5 d^3)}{2} [S(S+1) - \frac{25}{2}] \pm \frac{1}{20} S(S+1) t_B, \quad (18)$$

where \pm corresponds to two quantum superpositions $|\pm\rangle$ written in a spin representation as follows

$$|SM\rangle_{\pm} = \frac{1}{\sqrt{2}} (|\frac{5}{2} \frac{3}{2}; SM\rangle \pm |\frac{3}{2} \frac{5}{2}; SM\rangle), \quad (19)$$

with s - and p -type symmetry, respectively. It is worth noting that the bosonic double exchange contribution formally corresponds to ferromagnetic exchange coupling with $J_B = -\frac{1}{10}|t_B|$.

We see that the cumulative effect of the Heisenberg exchange and the bosonic double exchange results in a stabilization of the $S=4$ high-spin (ferromagnetic) state of the EH-dimer provided $|t_B| > 10J$ (see left panel in Fig. 1) and the $S=1$ low-spin ("ferrimagnetic") state otherwise (see right panel in Fig. 1). Spin states with intermediate S values: $S=2, 3$ correspond to a classical noncollinear ordering. It is interesting that for $|t_B| = 10J$ the energy of the dimer's S -type states does not depend on the value of the total spin, so that

we arrive at the surprising result of a 24-fold ($\sum_{S=1}^{S=4}(2S+1)$) degeneracy of the ground state of an isolated dimer (see central panel in Fig. 1).

To estimate the both quantities t_B and $J(d^5 d^3)$ and their dependence on the crystal structure parameters we can address the results of a comprehensive theoretical and experimental analysis of different superexchange integrals in perovskites RFeO_3 , RCrO_3 , and $\text{RFe}_{1-x}\text{Cr}_x\text{O}_3$ with Fe^{3+} and Cr^{3+} ions with electronic configurations d^5 and d^3 , respectively [40–42]. These perovskites are isostructural with many JT-magnets including $(\text{Ca},\text{Sr},\text{Ba})\text{FeO}_3$, RMnO_3 , $(\text{Ca},\text{Sr},\text{Ba})\text{RuO}_3$.

Antiferromagnetic kinetic exchange contribution to $J(e_g e_g)$ related with the e_g -electron transfer to partially filled e_g -shell can be written as follows [41, 42]

$$J(e_g e_g) = \frac{(t_{ss} + t_{\sigma\sigma} \cos \theta)^2}{2U}, \quad (20)$$

while for the d^5 - d^3 superexchange we arrive at a competition of the antiferromagnetic and ferromagnetic contributions

$$J_{FeCr} = J(d^5 d^3) = \frac{2}{15} \left(\frac{t_{\sigma\pi}^2}{U} \sin^2 \theta + \frac{t_{\pi\pi}^2}{U} (2 - \sin^2 \theta) \right) - \frac{\Delta E(35)}{10U} \left[\frac{(t_{ss} + t_{\sigma\sigma} \cos \theta)^2}{U} + \frac{t_{\sigma\pi}^2}{U} \sin^2 \theta \right]. \quad (21)$$

Here θ is the cation-anion-cation bonding angle, $t_{\sigma\sigma} > t_{\pi\sigma} > t_{\pi\pi} > t_{ss}$ are positive definite d - d transfer integrals, U is a mean d - d transfer energy (effective correlation energy), $\Delta E(35)$ is the energy separation between 3E_g and 5E_g terms for the $t_{2g}^3 e_g$ configuration.

Microscopically derived angular dependence of the superexchange integrals J_{FeFe} , J_{CrCr} , and J_{FeCr} does nicely describe the full set of experimental data on the value of T_N for various orthoferrites, orthochromites, mixed ferrites-chromites, as well as Mössbauer data on Fe-substituted orthochromites [40–42].

Figure 2 shows the dependence of the superexchange integrals $J_{FeCr} = J(d^5 d^3)$ and $J(e_g e_g)$ on the cation-anion-cation superexchange angle, typical for orthoferrites and orthochromites. The empty rectangles for $J(d^5 d^3)$ reproduce the experimental data [40] taking into account the measurement errors of the exchange integrals and the average values of the superexchange bonding angles. Dashed curve in Fig. 2 describes the angular dependence (20) for $J(e_g e_g)$ with quantitative estimates based on the analysis of the full set of experimental data on the value of exchange parameters for orthoferrites and orthochromites [40–42].

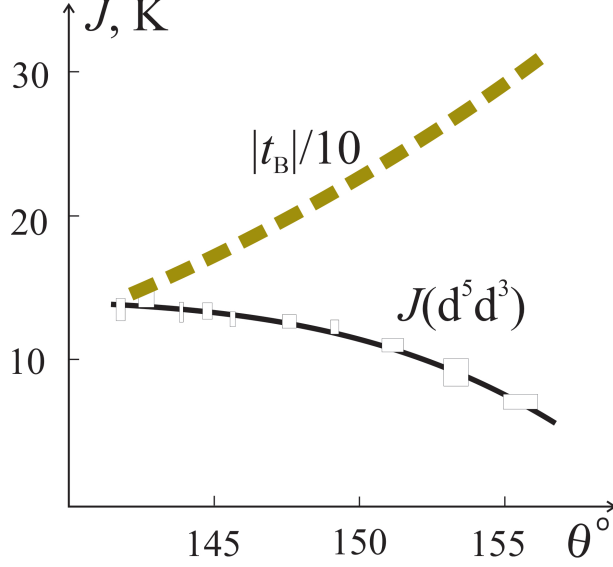


FIG. 2. (Color online) Angular dependence of $J(d^5 d^3)$ and $\frac{1}{10}|t_B|$ which define the effective integral $J_{eff} = J(d^5 d^3) - 0.1|t_B|$

The fitting allows us to predict the sign change for J_{FeCr} at $\theta_{cr} \approx 160-170^\circ$. In other words, the $(t_{2g}^3 e_g^2 - O^{2-} - t_{2g}^3)$ superexchange coupling becomes ferromagnetic at $\theta \geq \theta_{cr}$.

At variance with $J(d^5 d^3)$ the exchange parameter $J(e_g e_g) \approx |t_B|$ is shown to rapidly fall with the decrease in the bonding angle θ , so that at $\theta_{cr} \approx 142^\circ$ we come to compensation for the ferro- and antiferromagnetic contributions to the effective exchange parameter $J_{eff} = J(d^5 d^3) - 0.1|t_B|$ with $S = 1, 2, 3, 4$ degeneracy and a dramatic $S = 4 \rightarrow S = 1$ transformation of the spin ground state with tenfold reduction in the effective transfer integral of the composite boson (see Exp. (16)).

We believe that the results of the analysis of the angular dependence of the parameters $J(d^5 d^3)$ and $J(e_g e_g)$, presented in Fig. 2, can be used to analyze the spin structure of EH-dimers in JT magnets with a perovskite structure such as manganites, ferrates, and ruthenates (see Table 1).

So, for example, for the superexchange geometry, typical for LaMnO_3 [43] with the Mn-O-Mn bonding angle $\theta \approx 155^\circ$ we find $J(d^5 d^3) \approx +7 \text{ K}$ and $J(e_g e_g) \approx |t_B| \approx 297 \text{ K}$. In other words, for the effective exchange integral J_{eff} we come to a rather large value: $J_{eff} = J(d^5 d^3) - 0.1|t_B| \approx -23 \text{ K}$. Despite the antiferromagnetic sign of the Heisenberg superexchange integral these data unambiguously point to a dominant ferromagnetic contribution of the

bosonic double exchange mechanism with the ground ferromagnetic $S=4$ spin state for EH-dimer and maximal "nonreduced" value of the composite boson transfer integral.

For the bonding angle $\theta = 143^\circ$ typical for the heavy rare-earth manganites RMnO_3 (R=Dy, Ho, Y, Er) [43] the relation between $|t_B| \approx 154 \text{ K}$ and $J(d^5 d^3) \approx 14 \text{ K}$ [40] approaches to the critical one: $|t_B| = 10 J(d^5 d^3)$ evidencing a destabilization of the ferromagnetic state for the EH-dimers.

Thus, the structural factor plays a significant role for stabilization of one or another spin state of the EH-dimers and effective transfer integral for the composite boson. We believe that the change (decrease) in the angle of the cation-anion-cation superexchange bond with suppression of ferromagnetic interaction and metallicity can be the main reason for the strong effect of the substitution of Sr by Ca in JT magnets such as SrFeO_3 , SrRuO_4 , Sr_2RuO_4 , and $\text{Sr}_3\text{Ru}_2\text{O}_7$.

POSSIBLE PHASE STATES OF JT-MAGNETS WITH INSTABILITY TO CHARGE TRANSFER

In the limit of strong electron correlations and the prevalence of potential energy for valence electrons the charge-transfer-resistant stable "progenitor" JT-systems, as a rule, will be spin-magnetic insulators with a certain orbital ordering (OO) as a consequence of the cooperative JT effect. In the opposite limit of weak correlations and the prevalence of kinetic energy for valence electrons, we arrive at a system of itinerant electrons that form a Fermi liquid.

In the crossover CT-instability regime, instead of a single inactive charge d^n -component, the on-site Hilbert space of the d -centers includes a charge triplet of $d^n, d^{n\pm 1}$ -centers, which leads to the appearance of at least the eight parameters of diagonal and off-diagonal charge order [44]. Taking into account the spin degree of freedom and lattice modes, we arrive at a huge variety of possible phase states. The phase diagram's complexity originates from the specific crystal chemistry and a fine balance between the energies of the electron-lattice interaction, crystal field, local (Coulomb and exchange, or Hund) and nonlocal charge correlations, inter-site single and two-particle (composite boson) charge transfer, and spin-spin exchange. An inevitable consequence of the competition of many order parameters will be phase separation and the possibility of fine tuning of physical properties by changing

the chemical composition, applying external pressure, and going over to epitaxial films and heterostructures.

Taking into account the coexistence of one- and two-particle transport, the high-temperature disordered phase for such systems will be a kind of "boson-fermion soup" [45], or a "strange/bad" metal with a T -linear resistance dependence (strange metal) and a violation of the Mott-Ioffe-Regel criterion (bad metal). Indeed, the "strange/bad" metal behavior is common to practically all the JT-magnets listed in Table I.

One or another long-range order in JT magnets starts to form at high temperatures in a disordered phase, which is characterized by competition between the electron-lattice interaction, spin and charge fluctuations in the "struggle" for the low-temperature ground state. The local JT interaction leads to the stabilization of low-symmetry insulating magnetic structures. Low-energy charge fluctuations of the type of local anti-JT disproportionation reaction (1) depending on the ratio between the parameters of local and non-local correlations, the integrals of one- and two-particle transfer, and also the parameters of the electron-lattice interaction with a specific for electron-hole pairs breathing mode can lead to the formation of a wide variety of phases from charge (CO) and spin-charge ordering, collinear and noncollinear magnetic ordering, a coherent metallic Fermi-liquid FL phase, a bosonic superconductivity (BS) phase, and also specific nematic phase with the EH-dimer ordering [44, 46].

We believe that the expected superconductivity of JT-magnets is not a consequence of the BCS-type pairing, but the result of a quantum transport of the effective on-site composite electron/hole bosons. The superconducting state, as one of the possible ground states of JT magnets, can compete with the normal Fermi-liquid state, charge order, spin-charge density wave, collinear or noncollinear magnetic order, as well as specific quantum phases. The variety of competing phases clearly indicates the important role of phase separation effects [44, 47], which must be taken into account first of all when analyzing experimental data.

Below, without dwelling on a detailed analysis of phase states and phase diagrams, we consider only the main features of the single- and two-band JT-magnets in fully disproportionated state, when they form a system of spin-singlet or spin-triplet composite bosons in a nonmagnetic or magnetic lattice, respectively. Strictly speaking, to describe disproportionated systems, it is necessary to take into account the electron-lattice interaction, primarily

with the so-called breathing mode, but below we will consider the effective Hamiltonian of effective composite bosons in the "frozen" lattice approximation.

SINGLE-BAND JT-MAGNETS

Effective Hamiltonian of a system of spin-triplet composite bosons: non-magnetic lattice

As can be seen from Table 1 the anti-Jahn-Teller disproportionation in the system of tetrahedral JT centers with the configuration $3d^1$, $4d^1$, low-spin octa-centers with the configuration $3d^7$, $4d^7$ or octa-centers with configuration $3d^9$, $4d^9$ leads to the formation of a half-filled system of effective spin-triplet bosons moving in a non-magnetic lattice. We represent the Hamiltonian of such a system in the form as follows

$$\mathcal{H} = - \sum_{i>j,\nu} t_{ij} \left(\hat{B}_{i\nu}^\dagger \hat{B}_{j\nu} + \hat{B}_{i\nu} \hat{B}_{j\nu}^\dagger \right) + \sum_{i>j,\nu,\nu'} V_{ij} n_{i\nu} n_{j\nu'} - \sum_{i,\nu} \mu_\nu n_{i\nu} + \mathcal{H}_s, \quad (22)$$

where t_{ij} is the spin-independent boson transfer integral, V_{ij} is effective boson-boson repulsion (nonlocal correlations), μ is chemical potential, \mathcal{H}_s is spin Hamiltonian. The chemical potential μ is introduced to fix the boson concentration $n = \frac{1}{N} \sum_{i\nu} \langle \hat{n}_{i\nu} \rangle$.

The composite boson creation/annihilation operators $\hat{B}_{i\nu}^\dagger/\hat{B}_{i\nu}$, regardless of the spin component $\nu = 0, \pm 1$, obey the on-site anticommutation Fermi relations and the inter-site Bose commutation relations:

$$\{\hat{B}_i, \hat{B}_i^\dagger\} = 1, [\hat{B}_i, \hat{B}_j^\dagger] = 1. \quad (23)$$

The anticommutation Fermi relations can be rewritten as

$$[\hat{B}_i, \hat{B}_i^\dagger] = 1 - 2\hat{B}_i^\dagger \hat{B}_i = 1 - 2\hat{N}_i. \quad (24)$$

On the whole, these relations rule out the on-site double filling.

To take into account the influence of an external magnetic field, one can use the standard Peierls substitution

$$t_{ij} \rightarrow t_{ij} e^{i(\Phi_j - \Phi_i)}, \quad (25)$$

with

$$(\Phi_j - \Phi_i) = -\frac{q}{\hbar c} \int_{\mathbf{R}_i}^{\mathbf{R}_j} \mathbf{A}(\mathbf{r}) d\mathbf{l}, \quad (26)$$

where \mathbf{A} is the vector potential of a homogeneous magnetic field, the integration goes along the line connecting the sites i and j . In the general case spin Hamiltonian \mathcal{H}_s for the system of spin-triplet bosons can be represented as follows

$$\mathcal{H}_s = \sum_{i>j} J_{ij} (\hat{\mathbf{s}}_i \cdot \hat{\mathbf{s}}_j) + \sum_{i>j} j_{ij} (\hat{\mathbf{s}}_i \cdot \hat{\mathbf{s}}_j)^2 + K_{SIA} \sum_i (\mathbf{m}_i \cdot \hat{\mathbf{s}}_i) (\mathbf{n}_i \cdot \hat{\mathbf{s}}_i) + V_{TIA} - \sum_i (\mathbf{h} \cdot \hat{\mathbf{s}}_i), \quad (27)$$

where J_{ij} and j_{ij} are the bilinear and biquadratic isotropic exchange integrals, respectively, K_{SIA} is a constant, \mathbf{m} and \mathbf{n} are unit vectors that define two characteristic axes of the second-order single-ion anisotropy, V_{TIA} is two-ion bilinear and biquadratic anisotropy, \mathbf{h} is external field.

It is worth noting that the Cartesian form of the composite boson spin operator can be represented as follows

$$\hat{s}_\beta = \hat{B}_\alpha^\dagger \epsilon_{\alpha\beta\gamma} \hat{B}_\gamma, \quad (28)$$

where $\epsilon_{\alpha\beta\gamma}$ is Levi-Civita tensor, $\alpha, \beta, \gamma = x, y, z$.

In the paramagnetic region, Hamiltonian (27) actually reduces to the Hamiltonian of the well known lattice hard-core (*hc*) Bose system with an inter-site repulsion, governed in the nearest-neighbor approximation only by two parameters, t_B and V . At half-filling, depending on the relative values of the parameters, we arrive at a charge order (CO) or Bose-superfluid (BS) phase. As the temperature decreases, one or another magnetic order is realized in the system.

d^1, d^3 JT-magnets

Practically the only JT-magnets known in the literature with tetrahedral d^1 -centers, such as β - Sr_2VO_4 with V^{4+} and $(\text{Sr},\text{Ba})_3\text{Cr}_2\text{O}_8$ with Cr^{5+} , are considered to be typical insulators exhibiting Jahn-Teller distortions with orbital ordering and the formation of a system of weakly coupled spin dimers (see, e.g., Refs. [48–50]). We did not find any literature data on JT-magnets with tetrahedral d^3 -centers, except for the assumption made in Ref. [51] about the possibility of synthesizing $\text{Ba}_2\text{VGe}_2\text{O}_7$ melilite with V^{2+} ions, an anticipated JT-multiferroic.

The origin of the metal-to-insulator transition (MIT) in the series of rare-earth nickelates RNiO_3 with perovskite structure has challenged the condensed matter research community for almost three decades [52]. Furthermore, the recent theoretical prediction for superconductivity in LaNiO_3 thin films [53] has also triggered intensive research efforts.

The complex MIT phenomena in these materials are a perfect illustration of the competition between the potential and kinetic energy gain, presumably governed by structural factor, namely, the Ni-O-Ni bond angle, and clear evidence for strong electron-lattice effects, which have a dramatic effect on the character of the MIT.

Orthorhombic RNiO_3 ($\text{R} = \text{Pr}, \dots, \text{Lu}$) exhibit a first order metal-insulator phase transition to a charge ordered insulating state upon cooling below $T_{CO} = T_{MIT}$ spanning from 130 K for Pr to ~ 550 -600 K for heavy rare earths [52]. All these exhibit clear signatures of the charge disproportionated state with two types of Ni centers corresponding to alternating large $[\text{NiO}_6]^{10-}$ (Ni^{2+} center) and small $[\text{NiO}_6]^{8-}$ (Ni^{4+} center) octahedra strongly differing in magnetic moments ($\sim 2 \mu_B$ and ~ 0 , respectively) in full accordance with the disproportionation model (see Table I). At low temperatures ortho-nickelates show a magnetic phase transition toward an unusual antiferromagnetic structure defined by a propagation vector $(1/2, 0, 1/2)$ [52], which can be explained by a rather strong superexchange nnn (next-nearest neighbor) coupling of magnetic $S = 1$ Ni^{2+} centers. The largest anomaly at $T_{MIT} = T_N$ 130 K in PrNiO_3 was observed in the amplitude of the breathing mode, which undergoes a sharp jump of 0.15 \AA [54]. A further interesting observation is the existence of a nearly perfect linear correlation between the amplitude of the breathing mode associated to the charge order and the staggered magnetization below the MIT. In addition, the authors [54] suggest the existence of a hidden symmetry in the insulating phase, which may be related to a nematic contribution of bound EH dimers.

Increasing the Ni-O-Ni bond angle when moving from LuNiO_3 to LaNiO_3 leads to a gain in kinetic energy with a clear trend to a metallization due to two important effects, namely, an increase in the transfer integrals for the e_g -electrons and a decrease in the parameter V of inter-site repulsion (nonlocal correlations) due to an increase in the Ni-Ni separation. So, the x-ray diffraction, neutron scattering, transport, and thermodynamic experiments showed that globally rhombohedral single crystal LaNiO_3 samples revealed a

puzzlingly high metallicity, paramagnetic behavior down to 1.8 K [55] or some signatures of antiferromagnetic transition at 157 K [56] but no structural and metal-insulator transitions. Combined total neutron scattering and broadband dielectric spectroscopy experiments on polycrystalline samples [57] indicated that the structure of LaNiO_3 has a high degree of symmetry when viewed on long length scales, but similar to orthorhombic nickelates also has at least two different types of Ni sites when viewed locally. LaNiO_3 is locally distorted to orthorhombic at room temperature, and further to monoclinic at 200 K from globally rhombohedral structure [58]. This controversial behavior for LaNiO_3 can be the result of the peculiar "ortho-mono-rhombo" phase separation.

Another example of nickel JT-magnets is the quasi-2D nickelates ANiO_2 ($A = \text{Ag, Li, Na}$) which reveal existence of unconventional ground states stabilized by the frustrated triangular lattice geometry from a cooperative JT ordering of Ni^{3+} ions in NaNiO_2 to a *moderately charge ordering* $3\text{Ni}^{III+} \rightarrow \text{Ni}^{2+} + 2\text{Ni}^{3.5+}$ in antiferromagnetic metal AgNiO_2 [59]. In the case of LiNiO_2 there could be a competition between charge and orbital ordering, the nickel valency could be a mixture of 2+, 3+, and 4+ [60]. Comparison of NaNiO_2 with LiNiO_2 , where a number of different possible ground states are very close in energy, illustrates how two systems which are apparently so similar chemically, can nevertheless have very different behaviour [60].

d^9 JT-magnets

Isoelectronic quasi-2D cuprates and nickelates

The Cu^{2+} ion in octahedral complexes is characterized by the strongest JT bond and is the most popular, almost "textbook" illustration of the Jahn-Teller effect. The consequence of this effect is the formation of the dielectric state of a quantum antiferromagnet, for example, in KCuF_3 and La_2CuO_4 or quasi-2D ferromagnet K_2CuF_4 . However, in contrast to fluorides, in La_2CuO_4 the JT distortion leads to the formation of CuO_2 -planes with a "perovskite" configuration of CuO_4 -clusters with the ground $b_{1g} \propto d_{x^2-y^2}$ state of the e_g -hole, which provides a strong σ -coupling channel for hole transfer in the CuO_2 plane and disproportionation (2) to form spin- singlet and orbitally nondegenerate ($^1A_{1g}$) electronic $[\text{CuO}_4]^{7-}$ (analog of Cu^+ ion) and Zhang-Rice (ZR) [61] hole $[\text{CuO}_4]^{5-}$ (analog of the Cu^{3+}

ion) centers.

Recently [33, 44] we argued that there are no fundamental qualitative differences in the electronic structure of "apex-free" RNiO_2 nickelates and cuprates, primarily cuprates with a T' -structure. The unusual properties of cuprates and nickelates are the result of "competition" of various parameters that govern the ground state of the CuO_2 (NiO_2) planes. Thus, if for the vast majority of parent cuprates an antiferromagnetic dielectric phase is observed, which corresponds to the limit of strong local correlations, then this phase was not found in the parent nickelates RNiO_2 , which can be associated with a smaller value or even a change in the sign of the local correlation parameter. We have proposed [33, 44] to understand by "parent" cuprate or nickelate with hole half-filling of in-plane centers CuO_4 (NiO_4), which, depending on the parameters of local and non-local correlations, transfer integrals, exchange integrals, as well as the "external" crystal field formed by the out-of-plane environment, can have a different ground state - an antiferromagnetic insulator (AFMI), an unusual Bose superconductor (BS), a Fermi metal (FL) or a non-magnetic insulator with a charge ordering (CO). Obviously, these phases will differ not only in electronic but also in lattice degrees of freedom, the interaction of which ensures the minimum of the total free energy. In addition, the competition of several possible phases with similar energies will lead to phase separation, which will have a significant effect on the observed physical properties.

To describe the actual low-energy phase states of cuprate-nickelates, we proposed a minimal model for the $\text{CuO}_2/\text{NiO}_2$ -planes with the on-site Hilbert space reduced to a charge triplet of the three effective valence centers $[\text{CuO}_4]^{5-,6-,7-}/[\text{NiO}_4]^{6-,7-,8-}$ (nominally $\text{Cu}^{3+,2+,1+}/\text{Ni}^{2+,1+,0+}$) with different conventional spin, different orbital symmetry, and different local lattice configuration [33, 44, 62–66]. Making use of the $S = 1$ pseudospin formalism and the spin-pseudospin operators of the type of the Hubbard X -operators we have constructed the spin-pseudospin Hamiltonian of the charge triplet model, which takes into account local and nonlocal correlations, correlated one-particle and two-particle (bosonic) transport, and Heisenberg spin exchange. In particular cases the Hamiltonian reduces to the well-known "limiting" Hamiltonians (Hubbard, Heisenberg, atomic limit, hard-core bosons, ...). In accordance with experimental data for apexless cuprates [67], nickelates [68], and different typical cuprates we argue that antiferromagnetic insulating (AFMI), charge ordered (CO), Bose superconducting (BS), and Fermi-liquid (FL) phases are possible phase states of a model parent cuprate/nickelate, while typical phase states of doped systems, in particular,

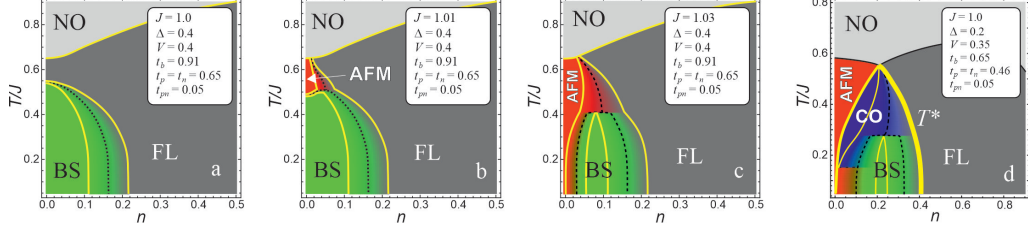


FIG. 3. (Color online) Model phase T - n -diagrams of hole-doped $\text{CuO}_2/\text{NiO}_2$ planes in cuprates/nickelates calculated in the effective field approximation ($n = p$ for hole doping) with the phase separation taken into account using Maxwell's construction; J is exchange integral, $\Delta = U/2$ local correlation parameter, V nonlocal correlation parameter, t_p, t_n, t_{pn} are three independent integrals of correlated single-particle transfer, t_B is the effective transfer integral of the composite boson (see insets) assuming competition between "monophases" NO (disordered), AFMI, BS, FL, CO. The boundaries between the phases represent lines of equal free energies. The dashed curves on (a)–(d) indicate the line of equal volume fractions of two neighboring phases, the yellow curves represent the lines of phase transitions of the "third" kind, limiting the regions with maximal 100% volume fraction of one of the phases. See Ref. [44] for detail. Let us pay attention to the strong change in the phase diagram even with a very small change in the parameters of the Hamiltonian (compare panels a, b, c).

mysterious pseudogap phase, are the result of a phase separation (PS). Superconductivity of cuprates/nickelates is not a consequence of pairing of doped holes [26], but the result of quantum transport of on-site composite hole bosons, whereas main peculiarities of normal state can be related to an electron-hole interplay for unusual Fermi-liquid phase and features of the PS. Puzzlingly, but it is the electron-lattice interaction, which in the BCS model determines s -wave pairing, in the model of local composite bosons gives $d_{x^2-y^2}$ -symmetry of the superconducting order parameter, thus showing once again a substantial involvement of the lattice in the HTSC. Within the framework of the effective field approximation, and the Maxwell construction, we have constructed a number of 2D T - p phase diagrams for the $\text{CuO}_2/\text{NiO}_2$ planes, which qualitatively reproduce main features of the experimentally observed 3D phase diagrams of cuprates and nickelates [44] (see Fig. 3). The pseudogap phase is associated with the PS region AFMI-CO-FL-BS, separated from the 100% FL-phase by the curve $T^*(p)$ of the "third order" phase transition.

In general, quasi-2B cuprates and nickelates provide an excellent example of the applica-

bility of the anti-JT disproportionation model. A large amount of experimental data from a long-term study of various properties of a wide class of old 2D cuprates and novel 2D nickelates, as well as the results of theoretical modeling of phase diagrams in the charge triplet model [44] provide important information about possible phase states of other JT magnets with charge transfer.

”Silver” JT-magnets

The anti-JT disproportionation model predicts the possibility of a ”silver or palladium path” to superconductivity in systems based on $\text{Ag}^{2+}(4d^9)$ or $\text{Pd}^+(4d^9)$, that is, the 4d analog of Cu^{2+} . The most likely candidate, silver fluoride AgF_2 [69–71], also known as $\alpha\text{-AgF}_2$, is an excellent analogue of cuprate with surprisingly close electronic parameters to La_2CuO_4 , but with greater deformation (buckling) of AgF_2 planes. However, this fluoride is a canted antiferromagnetic insulator, although close to a charge-transfer instability. Indeed, experimental studies [72] report the discovery of a metastable disproportionated diamagnetic phase $\beta\text{-AgF}_2$, interpreted as a charge-ordered compound $\text{Ag}^{1+}\text{Ag}^{3+}\text{F}_4$, which quickly transforms into the $\alpha\text{-AgF}_2$ structure.

Unlike the antiferromagnetic insulator Cu^{2+}O , its silver 4d analogue Ag^{2+}O is a diamagnetic semiconductor with a disproportionate Ag sublattice, whose chemical formula is often written as $\text{Ag}^{1+}\text{Ag}^{3+}\text{O}_2$ with O- $\text{Ag}^{1+}(4d^{10})$ -O collinear bonds and Ag^{3+} square planar bonds $(4d^8)\text{O}_4$ [73, 74]. In this case, the $[\text{AgO}_4]^{5-}$ cluster, like the $[\text{CuO}_4]^{5-}$ center in cuprates, is in a nonmagnetic state of the Zhang-Rice singlet type.

TWO-BAND JT MAGNETS

Single-band JT magnets, with their relatively simple electronic structure, provide an excellent illustration of the predictive power of the anti-JT disproportionation model, while the situation with two-band JT magnets is less certain.

Anti-Jahn-Teller disproportionation in ”two-band” systems of high-spin octa-centers with $3d^4$, $4d^4$ configuration or tetrahedral JT centers with $3d^6$, $4d^6$ configuration implies unusual phase with the coexistence of a half-filled system of effective spin-triplet electron or hole bosons with configuration $e_g^2 : {}^3A_{2g}$ or $\underline{e}_g^2 : {}^3A_{2g}$ and a magnetic lattice with the on-site

$S = 3/2$ configurations $t_{2g}^3 : ^4A_{2g}$, although this does not exclude the existence of unusual phases with delocalized t_{2g} -electrons (see review article [75]).

Two-band JT magnets include a large number of promising compounds, most of which are presented in the last column of Table I. Below, we briefly consider effective Hamiltonian, the features of the electronic structure and physical properties of the most prominent representatives of two-band JT magnets.

Effective Hamiltonian of a system of spin-triplet composite bosons: magnetic lattice

Anti-Jahn-Teller disproportionation in a system of high-spin octahedral JT-centers with $3d^4$, $4d^4$ configurations or tetrahedral JT-centers with $3d^6$, $4d^6$ configurations leads to the formation of a half-filled system of effective spin-triplet electron or hole bosons with configuration $e_g^2 : ^3A_{2g}$ or $\underline{e}_g^2 : ^3A_{2g}$, moving in a magnetic lattice with the on-site configurations $t_{2g}^3 : ^4A_{2g}$ (see Table I).

The effective Hamiltonian of such a system can also be represented as (22), however, with the spin-dependent composite boson transfer integral (see Exp. (16))

$$t_{ij} = \frac{S(S+1)}{20} t_B, \quad (29)$$

where $\hat{\mathbf{S}} = \hat{\mathbf{S}}_i + \hat{\mathbf{S}}_j$ is the total spin of the EH-pair (ij), $S = 1, 2, 3, 4$.

In contrast with the single-band JT-magnets the spin Hamiltonian \mathcal{H}_s for two-band JT-magnets will have a much more complex structure. Taking into account only the bilinear spin-spin isotropic exchange, it can be represented as follows

$$\mathcal{H}_s = \sum_{i>j} J_{ij}^{ll} (\hat{\mathbf{S}}_i \cdot \hat{\mathbf{S}}_j) + \sum_{i>j} J_{ij}^{bb} (\hat{\mathbf{s}}_i \cdot \hat{\mathbf{s}}_j) + \sum_{i>j} J_{ij}^{bl} (\hat{\mathbf{s}}_i \cdot \hat{\mathbf{S}}_j) + \sum_i J_{ii}^{bl} (\hat{\mathbf{s}}_i \cdot \hat{\mathbf{S}}_i), \quad (30)$$

where we assume the localized t_{2g} subshell. The first term describes the exchange interaction of the "lattice" spins, the second term describes the exchange interaction between spin-triplet bosons, the third and fourth terms describe the exchange between bosons and lattice spins, and the last term actually describes the intra-atomic Hund exchange. To fulfill Hund's rule, it is necessary to set the exchange integral J_{ii}^{bl} to be relatively large ferromagnetic.

Estimates for different superexchange couplings given the cation-anion-cation bond geometry typical for perovskites such as ferrates (Ca,Sr)FeO₃ or manganites RMnO₃ with bare octa-HS d^4 configurations [39] predict antiferromagnetic coupling for the nn lattice centers

($J^l > 0$) and for the two nearest neighbor bosons ($J^{bb} > 0$), whereas the coupling of the boson and the nearest neighbor lattice centers ($J^{bl} < 0$) can be ferro- or antiferromagnetic depending on the value of the cation-anion-cation bonding angle (see Fig. 1). Taking into account the boson transport which prefers an overall ferromagnetic ordering we arrive at a highly frustrated system with a competition of the ferro- and antiferromagnetic interactions.

Generally speaking, our model Hamiltonian describes the system that can be considered as a Bose-analogue of the *one orbital* double-exchange model system [76].

Chromium Cr²⁺ compounds

Among the JT chromium compounds, we have more or less reliable information about chromium difluoride CrF₂, according to which it is an antiferromagnetic insulator [77]. However, X-ray absorption and resonant inelastic x-ray scattering (RIXS) spectra of CrF₂ [78] point to a presence of three chromium oxidation states, namely Cr⁺, Cr²⁺, and Cr³⁺, which indicates instability with respect to charge transfer with clear signatures of the *d-d* disproportionation reaction in this JT magnet. The most likely explanation for this puzzle is phase separation, that is, the coexistence of antiferromagnetic regions and regions of a disproportionate phase.

Manganites RMnO₃

Features of the anti-JT disproportionation and its influence on the phase diagram of manganites RMnO₃ are considered in detail in Ref. [39].

A high-temperature thermally fluctuating charge disproportionated metallic state has been postulated for LaMnO₃ by different authors [79–81]. However, actually upon lowering the temperature one observes a first order phase transition at $T=T_{JT}$ ($T_{JT} \approx 750$ K in LaMnO₃) from the high-temperature fully disproportionated Bose metallic phase to a low-temperature orbitally ordered insulating phase with a cooperative Jahn-Teller ordering of the occupied e_g -orbitals of the Mn³⁺O₆ octahedra accompanied by A-type antiferromagnetic ordering below T_N ($T_N \approx 140$ K in LaMnO₃) [39, 81]. However, many experimental data point to a phase separation with the coexistence of insulating and disproportionated phases [39, 82].

The nonisovalent substitution and/or nonstoichiometry seems to revive the disproportionated phase and such manganites along with a metallic ferromagnetism with a colossal magnetoresistance reveal many properties typical for local spin-triplet superconductivity[39, 83–88].

Distinct signatures of high-temperature disproportionated phases are revealed also in other manganites, such as $\text{LaMn}_7\text{O}_{12}$ [89] with quadruple perovskite structure and YBaMn_2O_6 [90].

Iron Fe^{4+} JT magnets

All the ferrates listed in Table I, one way or another, are JT magnets that are unstable with respect to charge transfer.

The $\text{AFe}^{4+}\text{O}_3$ ($\text{A} = \text{Ca}, \text{Sr}, \text{Ba}$) perovskites show intriguing physical properties which are strongly dependent on the size and polarizability of the A-site ion since this affects all the main parameters governing their electronic structure.

With decreasing temperature orthorhombic metallic CaFeO_3 (CFO) exhibits a second-order phase transition to a narrow-gap semiconducting charge-ordered monoclinic semiconductor, or Hund’s insulator, with disproportionation into $\text{Fe}^{4\pm\delta}$ below a transition temperature $T_{CO} = T_{MIT} = 290 \text{ K}$ at ambient pressure, resulting in a three-dimensional rock salt type ordering of alternating small and large oxygen octahedra surrounding the nominal d^3 and d^5 Fe sites, respectively [91]. Parameter $\delta=0$ for $T \geq 290 \text{ K}$, it increases continuously with decreasing temperature below 290 K; typically δ approaches unity at low temperatures. The MIT is accompanied by the reduction of crystal symmetry as well as the sharp variation in electrical transport. Within our model the disproportionated phase in CFO implies the electron boson confinement in the larger FeO_6 octahedra.

The charge-disproportionation scenario for CFO has been well established experimentally using ^{57}Fe Mössbauer spectroscopy [92, 93], which clearly reveals two different sites with considerably different isomer shifts and hyperfine fields.

Let us pay attention to the possibility of the formation of domains in the charge-ordered state with 180° -domain walls, realizing the transition between two types of ”site-centered” charge order. At the center of the domain walls, a system of delocalized spin-triplet composite bosons with a ”bond-centered” charge order is formed, which formally corresponds

to the system of Fe^{4+} centers.

As temperature is lowered further, there is another transition in CFO from the paramagnetic to antiferromagnetic insulator at the Néel temperature $T_N \approx 120$ K. The low-temperature magnetic data can be fit equally well by a screw spiral structure or by a sinusoidal amplitude-modulated structure. The values of the moments at the two Fe sites are allowed to take different values; 2.5 and 3.5 μ_B for the spiral structure, and maximum amplitudes of 3.5 and 5.0 μ_B for the sinusoidal structure [91].

Note that the high-temperature orthorhombic metal phase of CFO can be viewed as a Hund's bad metal which appears as a mixed-valence state that fluctuates between two atomic configurations.

Different from the distorted perovskite CaFeO_3 undistorted cubic perovskites SrFeO_3 and BaFeO_3 keep metallic behaviors down to very low temperatures with different type of helical spin order. However, the ground state in these ferrates raises a lot of questions. At variance with Mössbauer data for CaFeO_3 the single magnetic hyperfine pattern for SrFeO_3 at 4 K indicates a rapid electron exchange between Fe^{3+} and Fe^{5+} ions, for the center shift and the hyperfine field coincide approximately with the average values of the corresponding parameters for CaFeO_3 [92]. In other words, "static" disproportionation occurs in CaFeO_3 with the formation of a site-centered charge order, whereas in SrFeO_3 we are dealing with "dynamic" disproportionation with the formation of a bond-centered charge order. Furthermore, experiments have revealed in SrFeO_3 a phase-separated state with a surprising variety of magnetic incommensurate helical and commensurate structures [94].

Surprisingly, a ferromagnetic ground state is found in BaFeO_3 single crystalline thin films with saturation magnetization and Curie temperature of 3.2 μ_B /formula unit and 115 K, respectively [95]. Unusually, for a uniform cubic ferromagnet, the films are insulating with an optical gap of ~ 1.8 eV.

An incommensurate helicoidal spin ordering observed both in CaFeO_3 and SrFeO_3 [96] up to very low temperatures can be explained as a result of a competition between conventional exchange coupling and the bosonic double exchange. Obviously, the theoretical and experimental study of the phase diagram for $(\text{Ca,Sr})\text{FeO}_3$ and substituted systems deserves further work, especially, aimed to a search of a possible superconductivity.

The ^{57}Fe Mössbauer measurements for the double-layered perovskite ferrate $\text{Sr}_3\text{Fe}_2\text{O}_7$ indicate the charge disproportionation and the magnetic properties, which are similar to

CaFeO₃ [97]. The critical temperature for the charge disproportionation reaction and the Néel temperature T_N of the helical spin order are determined to be ~ 343 K and ~ 120 K, respectively. Above 343 K, spectra clearly show a Fe⁴⁺ singlet. Puzzlingly, the spatial ordering pattern of the disproportionated charges has remained “hidden” to conventional diffraction probes, despite numerous x-ray and neutron scattering studies. Only recently making use of neutron Larmor diffraction and Fe K-edge resonant x-ray scattering Kim *et al.* [98] demonstrated checkerboard charge order in the FeO₂ layers and show that the “invisibility” of charge ordering in Sr₃Fe₂O₇ originates from frustration of the interactions between neighboring layers.

Less studied quasi-2D ferrate Sr₂FeO₄ with the K₂NiF₄ structure is a compound isotypic with the parent cuprate La₂CuO₄. It is antiferromagnetic semiconductor at ambient pressure with a Néel temperature T_N of about 56 K [99, 100]. Over the past 30 years, the concept of the electronic structure of Sr₂FeO₄ has changed from a Mott-type antiferromagnetic insulator similar to La₂CuO₄ [99] to a insulator with negative charge-transfer energy (negative- Δ_{pd}) [100], The insulating ground state of Sr₂FeO₄ is assumed to be stabilized by a hidden structural distortion similar to the charge order in the related Sr₃Fe₂O₇ and differs from the charge disproportionation in other Fe⁴⁺ oxoferrates.

However, we believe that, in fact, the ground spin-charge state in this ferrate, as well as in other JT ferrates, is determined by *d-d* anti-JT disproportionation. This is evidenced by the absence of a noticeable JT distortion of the FeO₆ octahedra, the manifestation of a phonon mode atypical for the K₂NiF₄ structure, which can be naturally associated with a breathing mode typical for *d-d* disproportionation, an elliptical cycloidal spin spiral structure typical of all JT ferrates, an insulator-metal transition under high pressure [100], For elucidating the details of the ground state we need further studies, in particular on single crystals of Sr₂FeO₄.

JT ruthenates

Just like Fe⁴⁺(3*d*⁴) JT ferrates, the Ru⁴⁺(4*d*⁴)-based ruthenates belong to the same family of the Ruddlesden-Popper (A_{*n*+1}B_{*n*}O_{3*n*+1}) compounds. They host a rich physics, including unconventional superconductivity in Sr₂RuO₄, a metamagnetic ground state in Sr₃Ru₂O₇, insulating antiferromagnetism in Ca₂RuO₄ and Ca₃Ru₂O₇, and both paramagnetic and fer-

romagnetic metallic states in CaRuO_3 and SrRuO_3 , respectively. Ruthenates undergo a variety of electronic, magnetic, and orbital ordering transitions, which are tunable with chemical doping, pressure, temperature, magnetic field, and epitaxial strain. However, their properties differ in many points from their 3d analogues. Not least, this is due to the fact that the 4d shell of the Ru^{4+} ion is more extended than the 3d shell of the Fe^{4+} electronic analog, which most likely leads to an increase in the crystal splitting parameter $10Dq$, a decrease in the local correlation parameter, and an increase in the transfer integrals. As a result the Ru^{4+} ($4d^{4+}$) ions tend to adopt a low-spin state or $S = 1$ state because relatively large crystal fields often overpower the Hund's rule coupling [101].

In other words, in ruthenates we seemingly encounter a fine high spin – low spin (HS – LS) balance up to the possibility of coexistence of HS- and LS-states [101, 102]. It means that by varying substitution, tuning the physical and chemical pressures, reducing the film thickness, one can observe different quantum states from typical for JT magnets as JT ferrates to states typical for low-spin t_{2g}^4 -systems with trend to a phase separation.

Practically all the layered ruthenates at low temperatures are characterized by a robust Fermi liquid behavior evidenced both by the quadratic temperature dependence of resistivity and by the observations of quantum oscillations. However, violation of the Mott-Ioffe-Regel limit for the basal plane resistivity and anomalous strange metallic behavior with a linear temperature dependence of resistivity at high temperature clearly reveal behavior inconsistent with any conventional Fermi-liquid paradigms [103] but typical for disproportionated systems with two types of the charge transport.

Ruthenates are an excellent candidate to explore the intricate interplay between structural and electron-spin degrees of freedom. For instance, Ca_2RuO_4 is a paramagnetic Mott insulator below the metal-insulator transition temperature $T_{MIT} \approx 360$ K with antiferromagnetic ordering below $T_N \approx 110$ K [104]. However, application of very modest pressures transforms it from an antiferromagnetic Mott insulator to a quasi 2D ferromagnetic metal. Under current flow, the insulating ground state was observed to transform into an electrically conducting phase with a high diamagnetic susceptibility.

Puzzlingly, the single crystalline Ca_2RuO_4 nanofilms exhibit co-appearance of high-temperature superconductivity with $T_c \approx 60$ K and ferromagnetism [105]. Such a high temperature of the superconducting transition testifies in favor of an unconventional mechanism of superconductivity of the type realized in high- T_c cuprates.

The replacement of Ca^{2+} ions (ionic radius 1.34 Å) with Sr^{2+} ions (ionic radius 1.44 Å) in bulk-family seemingly triggers a subtle modification in the electronic structure but a dramatic transformation of the ground state from antiferromagnetic insulating in Ca_2RuO_4 to superconducting and ferromagnetic in Sr_2RuO_4 with spiral spin structure in the ground normal metallic state [106].

Based on early Knight shift, polarized neutron scattering, muon-spin-resonance, and polar Kerr measurements, Sr_2RuO_4 has been widely thought to support a spin-triplet chiral p -wave superconducting state [107]. However, despite significant achievements in characterizing the properties of Sr_2RuO_4 over the last three decades, the precise nature of its electronic ground state and superconducting order parameter is still unresolved [108, 109]. Understanding the nature of superconductivity in Sr_2RuO_4 continues to be one of the most enigmatic problems in unconventional superconductivity despite vast interest, as well as a wide array of experiments performed on the material. Recent results have pushed the community towards potentially adopting an even-parity spin-singlet pairing state, although conventional states of this nature are not able to consistently explain all observations. It should be noted that superconductivity turns out to be a relatively common property of ruthenates, so very recently strain-stabilized superconductivity with $T_c \approx 2$ K was discovered in ruthenate RuO_2 films [110, 111].

Generally speaking, despite extensive efforts, a comprehensive understanding of electronic structure and physical properties in JT ruthenates is still lacking.

Iron-based superconductors

The Fe^{2+} iron based superconductors have a layered structure with conducting layers made of iron which are tetrahedrally coordinated by a pnictide or chalcogenide (As, Se, S or P), which are responsible for the superconductivity. These JT magnets exhibit the unprecedented richness of the physics, sometimes all within a single family – magnetism, unconventional superconductivity, quantum criticality, linear-in-T resistivity, nematic order, and a tendency toward orbital selective Mottness [112–115]. Researchers have found practically all phenomena associated with strongly correlated electron systems in the Fe-based materials. At the present time, a variety of theoretical approaches are being taken to understand these systems, although the issue remains to be fully settled.

We do not aim to give here a comprehensive review of the electronic structure and phase diagrams of iron based superconductors, but only pay attention to a number of specific features that allow us to assume an important role for the disproportionation mechanism. Superconductivity in FePn/Ch emerges out of a “bad-metal” normal state; and the superconducting phase occurs near antiferromagnetic order in proximity to a Mott transition. The parent iron pnictides are antiferromagnetically ordered metals, insulating behavior and AF order also appears in a variety of iron chalcogenides.

Unconventional non-BCS superconductivity in FePn/Ch has much in common with that of the copper oxides, in particular, the ratio of T_c versus the superfluid density is close to the Uemura plot as for the hole doped high- T_c cuprates [116, 117], as for cuprates the electronic nematicity has been observed in the normal state of many if not all the FePn/Ch.

At the same time, FePn/Ch are different in many respects from the cuprates. Thus, the high field inelastic neutron scattering data in the optimally doped Fe(Se,Te) superconductor [118] and in 112-type pnictide [119] show that similar to cuprates the magnetic fluctuations play a central role in iron superconductivity, however, these suggest that the superconductivity FePn/Ch is actually driven by a spin-triplet bound state. The spin-triplet nature of superconducting carriers in FePn/FeCh was proposed back in 2008 [28, 120] and confirmed by a number of experimental facts [121–123], although experimental data are contradictory [124, 125]. In this regard, let us turn our attention to one of the main modern technique for determining the spin of superconducting carriers - measuring the spin susceptibility by measuring the Knight shift [75]. It is believed that spins in a triplet superconductor should be polarized in an external magnetic field, just like free spins in an ordinary metal. Thus, in such a system one can expect that the spin susceptibility and the Knight shift should not have singularities in T_c . Spin anisotropy can suppress this for some directions but not for others. In a spin-singlet superconductor, the magnetic susceptibility vanishes at $T \rightarrow 0$. Thus, for spin-singlet superconductivity, a decrease in the uniform spin susceptibility below T_c can be expected, although qualitatively the same can occur for certain components of the triplet, although the vanishing susceptibility is often difficult to determine due to the background Van Vleck contribution. However, this technique does not take into account the complex nature of spin interactions and the spin structure of spin-triplet superconductors.

One way or another, the “singlet-triplet” dilemma for superconducting carriers in the vast majority of superconductors is considered within the framework of the BCS scenario,

while the model of anti-JT disproportionation in JT magnets represents a fundamentally different view of the mechanism of superconductivity, in which superconducting carriers are effective local, singlet or triplet, hole or electronic, composite bosons. By the way, our model assumes that superconducting carriers in FePn/Ch compounds consist of e_g -holes, and not of t_{2g} -electrons, as predicted by the single-electron multi-orbital band model [112].

At the moment, we cannot give an unambiguous conclusion about the role of the mechanism of anti-JT disproportionation in iron-based superconductors, however, in any case, finding the high- T_c superconductivity in the FePn/Ch compounds with the tetrahedral coordination of the iron $\text{Fe}^{2+}(3d^6)$ ions in HS state and its coexistence with an unconventional magnetism can be a key argument supporting the disproportionation scenario.

What seems even more surprising, our simple model gives convincing predictions of superconductivity and its features in different quasi-two-dimensional JT magnets, cuprates, nickelates, ruthenates, and ferropnictides/chalcogenides, differing both in the electronic structure of active centers, and in the local crystal structure. The model predicts hole-type bosonic spin-singlet superconductivity in 2D cuprates and nickelates, spin-triplet hole superconductivity in FePn/FeCh with sufficiently high T_c in both systems, and electronic superconductivity in Sr_2RuO_4 with very low T_c , by the way, in agreement with Hirsch's ideas about the hole nature of HTSC [126, 127].

CONCLUSION

We believe that unusual properties of a wide class of JT magnets, that is materials based on Jahn-Teller 3d and 4d ions with different crystal and electronic structures, from quasi-two-dimensional unconventional superconductors (cuprates, nickelates, ferropnictides/chalcogenides, ruthenate SrRuO_4), manganites with local superconductivity to 3D ferrates $(\text{CaSr})\text{FeO}_3$, nickelates RNiO_3 and silver oxide AgO with unusual charge and magnetic order can be explained within the framework of a single scenario, which assumes their instability with respect to anti-Jahn-Teller $d-d$ disproportionation. As a result of disproportionation, the parent ("progenitor") JT magnet is transformed into a half-filled system equivalent to a single- or two-band system of effective local composite spin-singlet or spin-triplet, electron or hole S -type bosons in a non-magnetic or magnetic lattice, which gives rise to an extremely rich set of phase states from non-magnetic and magnetic insulators,

unusual magnetic metallic and superconducting states, to a specific nematic ordering of the EH-dimers. Effective composite bosons cannot be considered as conventional quasiparticles, they are an indivisible part of many-electron configurations. Effective spin-dependent two-particle bosonic transport in two-band JT magnets results in a behavior typical for "double-exchange" systems.

The model provides a comprehensive understanding of the well established charge and magnetic order in JT ferrates and nickelates RNiO_3 including nontrivial effect of the cation-anion-cation bonding angle.

The most optimal conditions for HTSC with spin-singlet local composite bosons and a spinless lattice can only be achieved for low-symmetry quasi-two-dimensional d^9 JT magnets, such as 2D cuprates and nickelates, where disproportionation follows the traditional Jahn-Teller effect and orbital ordering.

The anti-JT disproportionation model points to a possibility of spin-triplet superconductivity in ruthenates Sr_2RuO_4 and RuO_2 , ferropnictides/chalcogenides FePn/FeCh , manganite LaMnO_3 , although in most of the known "candidates" ($\text{Ca}(\text{Sr})\text{FeO}_3$, RNiO_3 , AgO) one or another spin-charge order is realized. The model assumes that the effective superconducting carriers in the FePn/FeCh compounds consist of e_g holes rather than t_{2g} electrons, as predicted by the one-electron multi-orbital band models. The effective Hamiltonians for spin-triplet composite bosons in nonmagnetic and magnetic lattices have a complex spin structure, which must be taken into account when interpreting experiments to determine the spin of superconducting carriers.

I thank Dr Yuri Panov for the very fruitful multi-year collaboration, stimulating and encouraging discussions.

The research was supported by the Ministry of Education and Science of the Russian Federation, project No. FEUZ-2023-0017.

-
- [1] J.G. Bednorz, K.A. Müller, Possible high T_c superconductivity in the Ba-La-Cu-O system, *Z. Phys. B* 64 (1986) 189-193. <https://doi.org/10.1007/BF01303701>.
- [2] S.P. Ionov, G.V. Ionova, V.S. Lubimov, and E.F. Makarov, Instability of Crystal Lattices with Respect to Electron Density Redistributions, *Phys. Status Solidi B* 71 (1975) 11-57.

<https://doi.org/10.1002/pssb.2220710102>.

- [3] P.W. Anderson, Model for the Electronic Structure of Amorphous Semiconductors, *Phys. Rev. Lett.* 34 (1975) 953-955. <https://doi.org/10.1103/PhysRevLett.34.953>.
- [4] S. Scheurell, F. Scholz, T. Olesch, E. Kemnitz, ELECTROCHEMICAL EVIDENCE FOR Cu^{3+} - Cu^{2+} - Cu^{+} TRANSITIONS IN THE ORTHORHOMBIC $\text{YBa}_2\text{Cu}_3\text{O}_{7-x}$ PHASE, *Supercond. Sci. Technol.* 5 (1992) 303-305. <https://doi.org/10.1088/0953-2048/5/5/005>.
- [5] S. Larsson, Mixed valence model for superconductivity, *Brazilian Journal of Physics* 33 (2003) 744-749. <https://doi.org/10.1590/S0103-97332003000400022>.
- [6] J.A. Wilson, Again ‘why layered, square-planar, mixed-valent cuprates alone?’ - further pursuit of the ‘chemical’ negative-U route to the HTSC mechanism, *J. Phys.: Condens. Matter* 12 (2000) R517–R547. <https://iopscience.iop.org/article/10.1088/0953-8984/12/43/201>.
- [7] J.E. Hirsch and D.J. Scalapino, Double-valence-fluctuating molecules and superconductivity, *Phys. Rev. B* 32 (1985) 5639-5643. <https://doi.org/10.1103/PhysRevB.32.5639>.
- [8] A.W. Sleight, Oxide Superconductors: A Chemist’s View, *MRS Online Proceedings Library* 99 (1987) 3–8. <https://doi.org/10.1557/PROC-12-3>.
- [9] I.O. Kulik, A.G. Pedan, Phase transition in a model of superconducting glass, *Zh. Eksp. Teor. Fiz.* 79 (1980) 1469 [*Sov. Phys. JETP* 52 (1980) 742-748].
- [10] T.M. Rice and L. Sneddon, Real-Space and k-Space Electron Pairing in $\text{BaPb}_{1-x}\text{Bi}_x\text{O}_3$, *Phys. Rev. Lett.* 47 (1981) 689-692. <https://doi.org/10.1103/PhysRevLett.47.689>.
- [11] W.I.F. David, W.T.A. Harrison, J.M.F. Gunn *et al.*, Structure and crystal chemistry of the high- T_c superconductor $\text{YBa}_2\text{Cu}_3\text{O}_{7-x}$, *Nature London* 327 (1987) 310-312. <https://doi.org/10.1038/327310a0>.
- [12] C.M. Varma, Missing valence states, diamagnetic insulators, and superconductors, *Phys. Rev. Lett.* 61 (1988) 2713-2716. <https://doi.org/10.1103/PhysRevLett.61.2713>
- [13] I.E. Dzyaloshinskii, Chemical nature of the pairing of holes in high-temperature superconductors, *JETP Lett.* 49 (2) (1989) 142-144.
- [14] T.H. Geballe and B.Y. Mozyshes, Qualitative Understanding of the Highest T_c Cuprates, *Physica C* 341-348 (2000) 1821-1824. [https://doi.org/10.1016/S0921-4534\(00\)01112-6](https://doi.org/10.1016/S0921-4534(00)01112-6)
- [15] K.V. Mitsen and O.M. Ivanenko, Phase diagram of $\text{La}_{2-x}\text{M}_x\text{CuO}_4$ as the key to understanding the nature of high- T_c superconductors, *Phys. Usp.* 47 (2004) 493-510.
- [16] K.D. Tsendin, B.P. Popov, and D.V. Denisov, Explanation of the phase diagram of high-

- temperature superconductors in terms of the model of negative-U centres superconductivity, *Supercond. Sci. Technol.* **19** (2006) 313-318. <http://doi.org/10.1088/0953-2048/19/4/012>
- [17] Hiroshi Katayama-Yoshida, Koichi Kusakabe, Hidetoshi Kizaki, and Akitaka Nakanishi, General Rule and Materials Design of Negative Effective U System for High-Tc Superconductivity *Applied Physics Express* **1** (2008) 081703. <https://doi.org/10.1143/APEX.1.081703>.
- [18] Pouchard, M.; Villesuzanne, A. Are Superconductivity Mechanisms a Matter for Chemists? *Condens. Matter* **2020**, *5*, 67. <https://doi.org/10.3390/condmat5040067>
- [19] I. I. Mazin, D. I. Khomskii, R. Lengsdorf, J. A. Alonso, W. G. Marshall, R. M. Ibberson, A. Podlesnyak, M. J. Martínez-Lope, and M. M. Abd-Elmeguid, Charge Ordering as Alternative to Jahn-Teller Distortion, *Phys. Rev. Lett.* **98**, 176406 (2007).
- [20] R.A. Ogg Jr, Bose-Einstein Condensation of Trapped Electron Pairs. Phase Separation and Superconductivity of Metal-Ammonia Solutions, *Phys. Rev.* **69** (1946) 243-244. <https://doi.org/10.1103/PhysRev.69.243>.
- [21] M.R. Schafroth, Superconductivity of a Charged Ideal Bose Gas, *Phys. Rev.* **100** (1955) 463-475. <https://doi.org/10.1103/PhysRev.100.463>.
- [22] A.S. Alexandrov, High-Temperature Superconductivity: The Explanation, *Phys. Scr.* **83** (2011) 038301. <https://doi.org/10.1088/0031-8949/83/03/038301>.
- [23] K.A. Müller, The Polaronic Basis for High-Temperature Superconductivity, *J Supercond Nov Magn* **30** (2017) 3007-3018. <https://doi.org/10.1007/s10948-017-4262-7>.
- [24] D. Pavuna, G. Dubuis, A.T. Bollinger, J. Wu, X. He, I. Božović, On Local Pairs vs. BCS: Quo Vadis High-Tc Superconductivity, *J Supercond Nov Magn* **30** (2017) 731-734.
- [25] Božović, I.; He, X.; Wu, J.; Bollinger, A.T. Dependence of the Critical Temperature in Overdoped Copper Oxides on Superfluid Density. *Nature* **2016**, *536*, 309-311, [doi:10.1038/nature19061](https://doi.org/10.1038/nature19061).
- [26] Pelc, D.; Popcevic, P.; Pozek, M.; Greven, M.; Barišić, N. Unusual Behavior of Cuprates Explained by Heterogeneous Charge Localization. *Sci. Adv.* **2019**, *5*, eaau4538, [doi:10.1126/sciadv.aau4538](https://doi.org/10.1126/sciadv.aau4538).
- [27] Moskvin, A.S. Perspectives of Disproportionation Driven Superconductivity in Strongly Correlated 3d Compounds. *J. Phys.: Condens. Matter* **2013**, *25*, 085601, [doi:10.1088/0953-8984/25/8/085601](https://doi.org/10.1088/0953-8984/25/8/085601).
- [28] A.S. Moskvin, I. L. Avvakumov, Why does the tetrahedrally coordinated Fe drive the super-

- conductivity? Proc. III Int. Conf. "Fundamental Problems of High-Temperature Superconductivity" (Moscow, Zvenigorod, 13–17 October 2008) p. 215
- [29] Larsson, S. Strong electron correlation and phonon coupling in high T_c superconductors. *Physica C: Superconductivity* **2007**, 460-462, 1063–1065.
- [30] V. S. Vikhmin, S. E. Kapphan, Radiation Effects and Defects in Solids 157(6-12):853-856 (2002) DOI: 10.1080/10420150215821
- [31] S. Mazumdar, Negative charge-transfer gap and even parity superconductivity in Sr₂RuO₄, Phys. Rev. Research **2**, 023382 (2020).
- [32] R. J. Green, M. W. Haverkort, and G. A. Sawatzky, Bond disproportionation and dynamical charge fluctuations in the perovskite rare-earth nickelates, Phys. Rev. B **94**, 195127 (2016).
- [33] A.S. Moskvina, Charge transfer excitons in HTSC cuprates and nickelates, Optika i Spektroskopiya, **131** (4), 491 (2023) (in Russian)
- [34] C. Zener, Interaction between the d-Shells in the Transition Metals. II. Ferromagnetic Compounds of Manganese with Perovskite Structure, Phys. Rev. **82**, 403 (1951).
- [35] M. Merz, N. Nucker, S. Schuppler, D. Arena, J. Dvorak, Y.U. Idzerda, S.N. Ustinovich, A.G. Soldatov, S.V. Shiryayev and S.N. Barilo, X-ray absorption of Ba_{1-x}K_xBiO₃ and BaPb_{1-y}Bi_yO₃: Competition between bipolaronic and charge-density wave states, Europhys. Lett., **72**, 275 (2005).
- [36] C. Chailout, A. Santoro, J.P. Remeika, A.S. Cooper, G.P. Espinosa and M. Marezio, Bismuth valence order-disorder study in BaBiO₃ by powder neutron diffraction, Sol. St. Commun., **65**, 1363 (1988).
- [37] J. Rodríguez-Carvajal, M. Hennion, F. Moussa, A.H. Moudden, L. Pinsard, and A. Revcolevschi, Neutron-diffraction study of the Jahn-Teller transition in stoichiometric LaMnO₃, Phys.Rev. B **57**, R3189 (1998-II).
- [38] Q. Huang, A. Santoro, J.W. Lynn, R.W. Erwin, J.A. Borchers, J.L. Peng, and R.L. Greene, Structure and magnetic order in undoped lanthanum manganite, Phys. Rev. B **55**, 14987 (1997).
- [39] A. S. Moskvina, Disproportionation and electronic phase separation in parent manganite LaMnO₃, Phys. Rev. B **79**, 115102 (2009).
- [40] Moskvina, A.S., Ovanesyan, N.S., Trukhtanov, V.A. Angular dependence of the superexchange interaction Fe³⁺-O²⁻-Cr³⁺. Hyperfine Interact **1**, 265-281 (1975).

- [41] Moskvin, A. Structure–Property Relationships for Weak Ferromagnetic Perovskites. *Magnetochemistry* 2021, 7, 111. <https://doi.org/10.3390/magnetochemistry7080111>
- [42] A.S. Moskvin, Dzyaloshinskii Interaction and Exchange-Relativistic Effects in Orthoferrites, *JETP*, **132**, 517-547 (2021).
- [43] J. A. Alonso, M. J. Martínez-Lope, M. T. Casais, and M. T. Fernández-Díaz, Evolution of the Jahn-Teller Distortion of MnO₆ Octahedra in RMnO₃ Perovskites (R = Pr, Nd, Dy, Tb, Ho, Er, Y): A Neutron Diffraction Study, *Inorg. Chem.* **39**, 917 (2000).
- [44] A.S. Moskvin, Yu.D. Panov, Model of charge triplets for high- cuprates, *JMMM* **550**, 169004 (2022).
- [45] E. Pangburn, A. Banerjee, H. Freire, C. Pépin, Incoherent transport in a model for the strange metal phase: Memory-matrix formalism, [arXiv:2301.07125](https://arxiv.org/abs/2301.07125)
- [46] A. S. Moskvin, Yu. D. Panov, Nature of the Pseudogap Phase of HTSC Cuprates, *Physics of the Solid State*, **62**, 1554–1561 (2020).
- [47] A.S. Moskvin and Yu.D. Panov, Phase separation in high-T_c cuprates, *J. Phys.: Conf. Ser.* **2164**, 012014 (2022).
- [48] W. Gong, J. Greedan, G. Liu, and M. Bjorgvinsson, Crystal structure and magnetic properties of orthorhombic Sr₂VO₄ with tetrahedral vanadium(IV), *J. Solid State Chem.* **95**, 213 (1991).
- [49] J. Deisenhofer, S. Schaile, J. Teyssier, Zhe Wang, M. Hemmida, H.-A. Krug von Nidda, R. M. Eremina, M. V. Eremin, R. Viennois, E. Giannini, D. van der Marel, and A. Loidl, Electron spin resonance and exchange paths in the orthorhombic dimer system Sr₂VO₄, *Phys. Rev. B* **86**, 214417 (2012).
- [50] Zhe Wang, D. Kamenskyi, O. Cépas, M. Schmidt, D. L. Quintero-Castro, A. T. M. N. Islam, B. Lake, A. A. Aczel, H. A. Dabkowska, A. B. Dabkowski, G. M. Luke, Yuan Wan, A. Loidl, M. Ozerov, J. Wosnitza, S. A. Zvyagin, and J. Deisenhofer, High-field electron spin resonance spectroscopy of singlet-triplet transitions in the spin-dimer systems Sr₃Cr₂O₈ and Ba₃Cr₂O₈, *Phys. Rev. B* **89**, 174406 (2014).
- [51] Paolo Barone, Kunihiko Yamauchi, and Silvia Picozzi, Jahn-Teller distortions as a novel source of multiferroicity, *Phys. Rev. B* **92**, 014116 (2015).
- [52] Hepting, M. (2017). *The Rare-Earth Nickelates*. In: *Ordering Phenomena in Rare-Earth Nickelate Heterostructures*. Springer Theses. Springer, Cham.

- [53] J. Chaloupka, G. Khaliullin, Orbital Order and Possible Superconductivity in LaNiO₃/LaMO₃ Superlattices, *Phys. Rev. Lett.* **100**, 016404 (2008).
- [54] D. J. Gawryluk, Y. M. Klein, T. Shang, D. Sheptyakov, L. Keller, N. Casati, Ph. Lacorre, M. T. Fernández-Díaz, J. Rodríguez-Carvajal, and M. Medarde, Distortion mode anomalies in bulk PrNiO₃: Illustrating the potential of symmetry-adapted distortion mode analysis for the study of phase transitions, *Phys. Rev. B* **100**, 205137 (2019).
- [55] J. Zhang, H. Zheng, Y. Ren and J. F. Mitchell, High-Pressure Floating-Zone Growth of Perovskite Nickelate LaNiO₃ Single Crystals, *Cryst. Growth and Des.* **17**(5), 2730 (2017), doi:10.1021/acs.cgd.7b00205.
- [56] H. Guo, Z. W. Li, L. Zhao, Z. Hu, C. F. Chang, C. Y. Kuo, W. Schmidt, A. Piovano, T. W. Pi, O. Sobolev, D. I. Khomskii, L. H. Tjeng and A. C. Komarek, Antiferromagnetic correlations in the metallic strongly correlated transition metal oxide LaNiO₃, *Nat. Commun.* **9**, 43 (2018).
- [57] Shamblin, J., Heres, M., Zhou, H. et al. Experimental evidence for bipolaron condensation as a mechanism for the metal-insulator transition in rare-earth nickelates. *Nat Commun* **9**, 86 (2018). <https://doi.org/10.1038/s41467-017-02561-6>
- [58] B. Li, D. Louca, S. Yano, L. G. Marshall, J. Zhou and J. B. Goodenough, Insulating Pockets in Metallic LaNiO₃, *Adv. Electron. Mater.* **2**(2), 1500261 (2016), doi:10.1002/aelm.201500261, 1500261.
- [59] E. Wawrzynska, R. Coldea, E.M. Wheeler, I.I. Mazin, M.D. Johannes, T. Sorgel, M. Jansen, R.M. Ibberson, and P.G. Radaelli, Orbital degeneracy removed by charge order in triangular antiferromagnet AgNiO₂, *Phys. Rev. Lett.* **99** (2001) 157204.
- [60] Chen H.R., Freeman, C.L., Harding, J.H. (2011) Charge disproportionation and Jahn-Teller distortion in LiNiO₂ and NaNiO₂: A density functional theory study, *Physical Review B*, **84** (8), Article number: 085108
- [61] Zhang, F.C.; Rice, T.M. Effective Hamiltonian for the superconducting Cu oxides. *Physical Review B* **1988**, *37*, 3759–3761. DOI.org/10.1103/PhysRevB.37.3759
- [62] Moskvin, A.S. True Charge-Transfer Gap in Parent Insulating Cuprates. *Phys. Rev. B* **2011**, *84*, 075116, doi:10.1103/PhysRevB.84.075116.
- [63] Moskvin, A.S.; Panov, Yu.D. Topological Structures in Unconventional Scenario for 2D Cuprates. *J Supercond Nov Magn* **2019**, *32*, 61-84, doi:10.1007/s10948-018-4896-0.

- [64] Moskvin, A.S.; Panov, Yu.D. Electron-Hole Dimers in the Parent Phase of Quasi-2D Cuprates. *Phys. Solid State* **2019**, *61*, 1553-1558, doi:10.1134/S1063783419090178.
- [65] A. S. Moskvin, Large Variety of the On-Site Order Parameters and Phase States in Quasi-2D HTSC Cuprates, *Phys. Met. Metallogr.* **120**, 1252 (2019).
- [66] Moskvin, A.; Panov, Y. Effective-Field Theory for Model High-Tc Cuprates. *Condens. Matter* 2021, *6*, 24. <https://doi.org/10.3390/condmat6030024>
- [67] M. Naito, Y. Krockenberger, A. Ikeda, H. Yamamoto, Reassessment of the electronic state, magnetism, and superconductivity in high-Tc cuprates with the Nd₂CuO₄ structure, *Physica C* **523**, 28 (2016).
- [68] Li, D., Lee, K., Wang, B.Y. et al. Superconductivity in an infinite-layer nickelate. *Nature* **572**, 624–627 (2019). <https://doi.org/10.1038/s41586-019-1496-5>
- [69] P. Fischer, G. Roullet, D. Schwarzenbach, Crystal and magnetic structure of silver difluoride-II. Weak 4d-ferromagnetism of AgF₂, *J. Phys. Chem. Solids* **32**, 1641-1647 (1971).
- [70] Mariana Derzsi, Kamil Tokar, Przemyslaw Piekarczyk, and Wojciech Grochala, Charge ordering mechanism in silver difluoride, *Phys. Rev. B* **105**, L081113 (2022).
- [71] Nimrod Bachar, Kacper Koterwas, Jakub Gawraczynski *et al.*, Charge-Transfer and dd excitations in AgF₂, *Phys. Rev. Research* **4**, 023108 (2022).
- [72] C. Shen, B. Zemva, G.M. Lucier, O. Graudejus, J.A. Allman, and N. Bartlett, Disproportionation of Ag(II) to Ag(I) and Ag(III) in Fluoride Systems and Syntheses and Structures of (AgF⁺)₂AgF₄-MF₆- Salts (M = As, Sb, Pt, Au, Ru), *Inorg. Chem.* **38**, 4570-4577 (1999).
- [73] Vladimiro Scatturin, Pier Luigi Bellon and Alvin J. Salkind, The Structure of Silver Oxide Determined by Means of Neutron Diffraction, *J. Electrochem. Soc.* **108**, 819-822 (1961).
- [74] Jeremy P. Allen, David O. Scanlon, and Graeme W. Watson, Electronic structures of silver oxides, *Phys. Rev. B* **84**, 115141 (2011).
- [75] P. J. Hirschfeld, Using gap symmetry and structure to reveal the pairing mechanism in Fe-based superconductors, *Comptes Rendus Physique* **17**, 197 (2016).
- [76] Dong, S., Yu, R., Yunoki, S. et al. Double-exchange model study of multiferroic RMnO₃ perovskites. *Eur. Phys. J. B* **71**, 339–344 (2009). <https://doi.org/10.1140/epjb/e2009-00225-1>
- [77] J. W. Stout, Phillip DeLassus; CrF₂, A CANTED ANTIFERROMAGNET. *AIP Conference Proceedings* 1 March 1972; **5** (1): 669. <https://doi.org/10.1063/1.3699510>

- [78] J. Jiménez-Mier, P. Olalde-Velasco, W.-L. Yang, and J. Denlinger, X-ray absorption and resonant inelastic x-ray scattering (RIXS) show the presence of Cr⁺ at the surface and in the bulk of CrF₂, AIP Conference Proceedings **1671**, 020002 (2015).
- [79] R. Raffaele, H. U. Anderson, D.M. Sparlin, and P.E. Parris, Transport anomalies in the high-temperature hopping conductivity and thermopower of Sr-doped La(Cr,Mn)O₃, Phys. Rev. B **43**, 7991 (1991).
- [80] J.A.M. Van Roosmalen and E.H.P. Cordfunke, The Defect Chemistry of LaMnO₃+delta: 4. Defect Model for LaMnO₃+delta, J. Solid State Chem. **110**, 109-112 (1994).
- [81] J.-S. Zhou and J. B. Goodenough, Paramagnetic phase in single-crystal LaMnO₃, Phys. Rev. B **60**, R15002 (1999); Orbital order-disorder transition in single-valent manganites, Phys. Rev. B **68**, 144406 (2003).
- [82] C. Ritter, M.R. Ibarra, J.M. De Teresa, P.A. Algarabel, C. Marquina, J. Blasco, J. Garcia, S. Oseroff, and S-W. Cheong, Influence of oxygen content on the structural, magnetotransport, and magnetic properties of LaMnO₃+delta, Phys. Rev. B **56**, 8902 (1997).
- [83] Kim Yong-Jihn, P-wave Pairing and Colossal Magnetoresistance in Manganese Oxides, Mod. Phys. Lett. B **12**, 507 (1998).
- [84] V.N. Krivoruchko, Local spin-triplet superconductivity in half-metallic manganites: A perspective platform for high-temperature topological superconductivity, Low Temperature Physics **47**, 901 (2021).
- [85] V. Markovich, I. Fita, A. Wisniewski, R. Puzniak, D. Mogilyansky, L. Titelman, L. Vradman, M. Herskowitz, and G. Gorodetsky, Metastable diamagnetic response of 20nm La_{1-x}MnO₃ particles, Phys. Rev. B **77**, 014423 (2008).
- [86] M. Kasai, T. Ohno, Y. Kauke, Y. Kozono, M. Hanazono, and Y. Sugita, Jpn. J. Appl. Phys. **29**, L2219 (1990).
- [87] A.V. Mitin, G.M. Kuz'micheva, and S.I. Novikova, Complex oxides based on manganese with a perovskite structure and its derivative, Russian Journal of Inorganic Chemistry **42**, 1791 (1997).
- [88] R. Nath, A.K. Raychaudhuri, Ya.M. Mukovskii, P. Mondal, D. Bhattacharya, and P. Mandal, Electric field driven destabilization of the insulating state in nominally pure LaMnO₃, J Phys Condens Matter **25** (15), 155605 (2013).
- [89] Cabassi R Bolzoni F Gilioli E Bissoli F Prodi A and Gauzzi A Jahn-Teller-induced crossover

- of the paramagnetic response in the singly valent eg system LaMn₇O₁₂, 2010 Phys. Rev. B **81** 214412
- [90] Schaile S Krug von Nidda H-A Deisenhofer J Loidl A Nakajima T and Ueda Y Korringa-like relaxation in the high-temperature phase of A-site ordered YBaMn₂O₆, 2012 Phys. Rev. B **85** 205121
- [91] P. M. Woodward, D. E. Cox, E. Moshopoulou, A. W. Sleight, and S. Morimoto, Structural studies of charge disproportionation and magnetic order in CaFeO₃, Phys. Rev. B **62**, 844 (2000).
- [92] M. Takano, N. Nakanishi, Y. Takeda, S. Naka, T. Takada, Charge disproportionation in CaFeO₃ studied with the Mössbauer effect, Materials Research Bulletin, **12**, 923-928 (1977),
- [93] T. Takeda, R. Kanno, Y. Kawamoto, M. Takano, S. Kawasaki, T. Kamiyama, and F. Izumi, Metal-semiconductor transition, charge disproportionation, and low-temperature structure of Ca_{1-x}Sr_xFeO₃ synthesized under high-oxygen pressure, Solid State Sci. **2**, 673 (2000).
- [94] M. Reehuis, C. Ulrich, A. Maljuk, Ch. Niedermayer, B. Ouladdiaf, A. Hoser, T. Hofmann, and B. Keimer, Neutron diffraction study of spin and charge ordering in SrFeO_{3-d}, Phys. Rev. B **85**, 184109 (2012).
- [95] S. Chakraverty, T. Matsuda, N. Ogawa, H. Wadati, E. Ikenaga, M. Kawasaki, Y. Tokura, and H. Y. Hwang, "BaFeO₃ cubic single crystalline thin film: A ferromagnetic insulator", Appl. Phys. Lett. 103, 142416 (2013) <https://doi.org/10.1063/1.4824210>
- [96] J. Fujioka, S. Ishiwata, Y. Kaneko, Y. Taguchi, and Y. Tokura, Variation of charge dynamics upon the helimagnetic and metal-insulator transitions for perovskite AFeO₃ (A = Sr and Ca), Phys. Rev. B **85** (2012) 155141. <https://doi.org/10.1103/PhysRevB.85.155141>.
- [97] K. Kuzushita, S. Morimoto, S. Nasu and S. Nakamura, Charge Disproportionation and Antiferromagnetic Order of Sr₃Fe₂O₇, J. Phys. Soc. Jpn., **69** 2767 (2000).
- [98] J.-H. Kim, D. C. Peets, M. Reehuis, P. Adler, A. Maljuk, T. Ritschel, M. C. Allison, J. R. L. Mardegan, J. Geck, P. J. Bereciartua Perez, S. Francoual, A. C. Walters, T. Keller, P. M. Abdala, P. Pattison, P. Dosanjh, and B. Keimer, Hidden Charge Order in an Iron Oxide Square Lattice Compound, Phys. Rev. Lett. **127**, 097203 (2021).
- [99] P. Adler, Properties of K₂NiF₄-type Oxides Sr₂FeO₄, J. Solid State. Chem. **108**, 275 (1994).
- [100] Peter Adler, Manfred Reehuis, Norbert Stuesser, Sergey A. Medvedev, Michael Nicklas, et al.. Spiral magnetism, spin flop, and pressure-induced ferromagnetism in the negative charge-

- transfer-gap insulator Sr₂FeO₄. *Phys. Rev. B* **105**, 054417 (2022).
- [101] M. Itoh, M. Shikano, and T. Shimura, High- and low-spin transition of Ru⁴⁺ in the perovskite-related layered system Sr_{n+1}Ru_nO_{3n+1}, $n = 1, 2$, and ∞ with changes in n , *Phys. Rev. B* **51**, 16432 (1995).
- [102] A. J. Grutter, F. J. Wong, E. Arenholz, A. Vailionis, and Y. Suzuki, Evidence of high-spin Ru and universal magnetic anisotropy in SrRuO₃ thin films, *Phys. Rev. B* **85**, 134429 (2012).
- [103] G. Cao, W.H. Song, Y.P. Sun, X.N. Lin, Violation of the Mott-Ioffe-Regel limit: high-temperature resistivity of itinerant magnets Sr_{n+1}Ru_nO_{3n+1} ($n=2,3,\infty$) and CaRuO₃, *Solid State Communications*, **131**, 331-336 (2004).
- [104] S. Nakatsuji and Y. Maeno, Quasi-Two-Dimensional Mott Transition system Ca_{2-x}Sr_xRuO₄, *Phys. Rev. Lett.* **84**, 2666 (2000).
- [105] Nobukane, H., Yanagihara, K., Kunisada, Y. et al. Co-appearance of superconductivity and ferromagnetism in a Ca₂RuO₄ nanofilm crystal. *Sci Rep* **10**, 3462 (2020). <https://doi.org/10.1038/s41598-020-60313-x>.
- [106] Y. Maeno, H. Hashimoto, K. Yoshida, S. Nishizaki, T. Fujita, J.G. Bednorz, and F. Lichtenberg, Superconductivity in a layered perovskite without copper, *Nature (London)* **372** 532-534 (1994). <https://doi.org/10.1038/372532a0>.
- [107] A.P. Mackenzie and Y. Maeno, The superconductivity of Sr₂RuO₄ and the physics of spin-triplet pairing, *Rev. Mod. Phys.* **75**, 657-712 (2003). <https://doi.org/10.1103/RevModPhys.75.657>.
- [108] A.P. Mackenzie, T. Scaffidi, C.W. Hicks, and Y. Maeno, Even odder after twenty-three years: the superconducting order parameter puzzle of Sr₂RuO₄, *npj Quantum Mater.* **2** 40-49 (2017). <https://doi.org/10.1038/s41535-017-0045-4>.
- [109] A. J. Leggett, Y. Liu, Symmetry Properties of Superconducting Order Parameter in Sr₂RuO₄, *J Supercond Nov Magn* **34**, 1647 (2021).
- [110] Ruf, J.P., Paik, H., Schreiber, N.J. et al. Strain-stabilized superconductivity. *Nat Commun* **12**, 59 (2021). <https://doi.org/10.1038/s41467-020-20252-7>
- [111] M. Uchida, T. Nomoto, M. Musashi, R. Arita, and M. Kawasaki, Superconductivity in Uniquely Strained RuO₂ Films, *Phys. Rev. Lett.* **125**, 147001 (2020).
- [112] G. R. Stewart, Superconductivity in iron compounds, *Rev. Mod. Phys.* **83**, 1589 (2011).
- [113] Andrey Chubukov, Peter J. Hirschfeld; Iron-based superconductors, seven years later. *Physics*

- Today 1 June 2015; 68 (6): 46–52. <https://doi.org/10.1063/PT.3.2818>
- [114] Qimiao Si, Rong Yu, Elihu Abrahams, High Temperature Superconductivity in Iron Pnictides and Chalcogenides, *Nature Rev. Mater.* **1**, 16017 (2016).
- [115] Kreisel, A.; Hirschfeld, P.J.; Andersen, B.M. On the Remarkable Superconductivity of FeSe and Its Close Cousins. *Symmetry* 2020, 12, 1402. <https://doi.org/10.3390/sym12091402>
- [116] J.P. Carlo, Y.J. Uemura, T. Goko, G.J. MacDougall, J.A. Rodriguez, W. Yu, G.M. Luke, Pengcheng Dai, N. Shannon, S. Miyasaka, S. Suzuki, S. Tajima, G.F. Chen, W.Z. Hu, J.L. Luo, N.L. Wang, Static Magnetic Order and Superfluid Density of RFeAs(O,F) (R=La,Nd,Ce) and LaFePO Studied by Muon Spin Relaxation: Unusual Similarities with the Behavior of Cuprate Superconductors, *Phys. Rev. Lett.* **102**, 087001 (2009).
- [117] A. Adamski, C. Krellner, M. Abdel-Hafiez, Signature of multigap nodeless superconductivity in fluorine-doped NdFeAsO, *Phys. Rev. B*, **96**, 100503(R) (2017).
- [118] Juanjuan Liu et al. A Triplet Resonance in Superconducting Fe_{1.03}Se_{0.4}Te_{0.6}, *Chinese Phys. Lett.* **35** 127401 (2018).
- [119] Tao Xie, Dongliang Gong, Haranath Ghosh, Abyay Ghosh, Minoru Soda, Takatsugu Masuda, Shinichi Itoh, Frédéric Bourdarot, Louis-Pierre Regnault, Sergey Danilkin, Shilian Li, and Huiqian Luo, Neutron Spin Resonance in the 112-Type Iron-Based Superconductor, *Phys. Rev. Lett.* **120**, 137001 (2018).
- [120] Patrick A. Lee and Xiao-Gang Wen, Spin-triplet p-wave pairing in a three-orbital model for iron pnictide superconductors, *Phys. Rev. B* **78**, 144517 (2008).
- [121] S.-H. Baek, H.-J. Grafe, F. Hammerath, M. Fuchs, C. Rudisch, L. Harnagea, S. Aswartham, S. Wurmehl, J. van den Brink and B. Büchner, 75As NMR-NQR study in superconducting LiFeAs, *Eur. Phys. J. B* **85** 159 (2012).
- [122] Torben Hänke, Steffen Sykora, Ronny Schlegel, Danny Baumann, Luminita Harnagea, Sabine Wurmehl, Maria Daghofer, Bernd Büchner, Jeroen van den Brink, and Christian Hess, Probing the Unconventional Superconducting State of LiFeAs by Quasiparticle Interference, *Phys. Rev. Lett.* **108**, 127001 (2012).
- [123] P. M. R. Brydon, Maria Daghofer, Carsten Timm, and Jeroen van den Brink, Theory of magnetism and triplet superconductivity in LiFeAs, *Phys. Rev. B* **83**, 060501(R) (2011).
- [124] J. Brand, A. Stunault, S. Wurmehl, L. Harnagea, B. Büchner, M. Meven, and M. Braden, Spin susceptibility in superconducting LiFeAs studied by polarized neutron diffraction, *Phys.*

- Rev. B **89**, 045141 (2014).
- [125] J.A. Gifford, B.B. Chen, J. Zhang *et al.*, Determination of spin polarization using an unconventional iron superconductor, AIP Advances **6**, 115023 (2016).
- [126] J.E. Hirsch, Proc. SPIE 10105, Oxide-based Materials and Devices VIII, 101051V (7 March 2017).
- [127] J.E. Hirsch, F. Marsiglio, Understanding electron-doped cuprate superconductors as hole superconductors, Physica C: Superconductivity and its Applications **564**, 29-37 (2019) .

TABLE I. $3d^n$ and $4d^n$ JT-magnets.

JT-configuration JT ions	Symm.	LS/HS	Local boson	Lattice	Representative compounds
$3d^1(e_g^1):^2E$ Ti ³⁺ , V ⁴⁺ , Cr ⁵⁺	tetra	-	$e_g^{2,3}A_{2g}$ s=1	A_{1g} S=0	β -Sr ₂ VO ₄ (Sr,Ba) ₃ Cr ₂ O ₈
$3d^3(e_g^3):^2E$ V ²⁺ , Cr ³⁺ , Mn ⁴⁺	tetra	LS	$\underline{e}_g^{2,3}A_{2g}$ s=1	A_{1g} S=0	Ba ₂ VGe ₂ O ₇ (?)
$3d^4(t_{2g}^3e_g^1):^5E$ Cr ²⁺ , Mn ³⁺ , Fe ⁴⁺	octa	HS	$e_g^{2,3}A_{2g}$ s=1	A_{2g} S=3/2	CrO, CrF ₂ Sr ₂ FeO ₄ (Ca,Sr,Ba)FeO ₃ (Ca,Sr,Ba) ₃ Fe ₂ O ₇ RMnO ₃ , LaMn ₇ O ₁₂
$4d^4(t_{2g}^3e_g^1):^5E$ Ru ⁴⁺	octa	HS	$e_g^{2,3}A_{2g}$ s=1	A_{2g} S=3/2	(Ca,Sr) ₂ RuO ₄ (Ca,Sr)RuO ₃ , RuO ₂ (Ca,Sr) ₃ Ru ₂ O ₇
$3d^6(e_g^3t_{2g}^3):^5E$ Fe ²⁺ , Co ³⁺	tetra	HS	$\underline{e}_g^{2,3}A_{2g}$ s=1	A_{2g} S=3/2	FePn, FeCh, Na ₅ CoO ₄
$3d^7(t_{2g}^6e_g^1):^2E$ Co ²⁺ , Ni ³⁺	octa	LS	$e_g^{2,3}A_{2g}$ s=1	A_{1g} S=0	RNiO ₃ (Li,Na,Ag)NiO ₂
$3d^9(t_{2g}^6e_g^3):^2E$ Cu ²⁺ , Ni ⁺	octa	-	$\underline{e}_g^{2,3}A_{2g}$ s=1	A_{1g} S=0	CuF ₂ , KCuF ₃ , K ₂ CuF ₄
$4d^9(t_{2g}^6e_g^3):^2E$ Pd ⁺ , Ag ²⁺	octa	-	$\underline{e}_g^{2,3}A_{2g}$ s=1	A_{1g} S=0	AgO (Ag ¹⁺ Ag ³⁺ O ₂)
$3d^9(t_{2g}^6e_g^3):^2B_{1g}$ Cu ²⁺ , Ni ⁺	octa* square	-	$b_{1g}^2:1A_{1g}$ s=0	A_{1g} S=0	HTSC cuprates RNiO ₂ , CuO
$4d^9(t_{2g}^6e_g^3):^2B_{1g}$ Pd ⁺ , Ag ²⁺	octa* square	-	$b_{1g}^2:1A_{1g}$ s=0	A_{1g} S=0	AgF ₂ , KAgF ₃ Cs ₂ AgF ₄ , LaPdO ₂ (?)